MODELING OF RING RESONATOR AS AN OPTICAL FILTER USING MEEP SOFTWARE

BY

MATERE MANYONGE ISAAC

A THESIS SUBMITTED IN PARTIAL FULFILLMENT OF THE REQUIREMENTS FOR THE DEGREE OF MASTER OF SCIENCE IN PHYSICS, SCHOOL OF SCIENCE

UNIVERSITY OF ELDORET, ELDORET KENYA.

2016

DECLARATION

Declaration by the Candidate

This thesis is my original work and has not been submitted for any academic award in any University or Institution. It shall not be reproduced in part or full, or in any format without prior written permission from the author and/or University of Eldoret.

Matere Manyonge Isaac Signature: _____ Date: _____

SC/PGP/005/12

APPROVAL BY THE SUPERVISORS

This thesis has been submitted with our approval as University Supervisors.

Dr David W. Waswa Signature:_____ Date: _____

University of Eldoret,

Department of Physics

Prof Joel K. Tonui Signature:_____ Date: _____

University of Eldoret,

Department of Physics

DEDICATION

This thesis is dedicated to the Matere's Family, mentors, relatives and friends

ACKNOWLEDGEMENT

I thank the University of Eldoret and the Department of Physics for the use of its facilities. I acknowledge my supervisors, Dr. David W. Waswa and Prof Joel K. Tonui for offering me an opportunity to work under them, and being always available for support and guidance throughout this work. I also thank Prof. Filip Dominec of the Institute of Physics, Academy of Sciences of the Czech Republic for the assistance rendered during this work. I express my gratitude to the family of Jesse Matere and Damara Matere. Thank you for your assistance. I also thank Pancy Kimutai for her support and encouragement. I thank the members of the Fibre optics Group University of Eldoret for sharing their experience and for providing a cheerful atmosphere in the laboratory. I thank my brothers and sister, for being helpful during the period of my study. Last but not least I acknowledge all of the rest of my friends for whatever support and encouragement they accorded me during my study period, I really appreciate them.

ABSTRACT

Ring resonators are key components in modern optical networks. Their small size allows high density integration in optical photonic circuits due to the use of high index contrast. Ring resonator filters based Optical Filters for wavelength division multiplexing (WDM) are considered as one example in this technology. This thesis is a simulation study of Ring resonators which are widely used for various applications such as Optical antennas, Optical bandpass filters, Optical couplers and Optical oscillators. The description, design, simulation and layout of a ring resonator were carried out using Mit Electromagnetic Equation Propagation (MEEP) software. Coupling a closed loop resonator with a straight waveguide using evanescent coupling leads to a filter behavior of a new structure. By using the MEEP software, the transfer functions provide detailed physical interpretations of the resonator which are required to design good filter characteristics. Some of the characteristics include the Free Spectral Range (FSR), Finesse (F) and Quality factor (Q). The ring resonator modeled achieved a resonant frequency of 1.45518 x 10^{15} rad/s and resonance wavelength of 1.2955 μm, a single mode of 0.15076 GHz frequency was also achieved that resulted in a single mode source which is analytically solvable. Change in dielectric constant of the ring and perfect matched layers reduced greatly the power transmitted in the waveguide; hence leading to the downward shifting of the power. In addition an increase in length between the ring and the waveguide led to a decrease in the power coupled in the ring. A horizontal decrease in power was eminent when the computation cell and number of rings were increased from a single ring to triple rings. Vertical decrease in power and horizontal shifting of power coupled in the ring resonator were also achieved; which are the characteristics of fixed and tunable filters respectively. These research findings will help greatly in improving data and signal selection in communication as the process increase the speed of communication.

TABLE OF CONTENTS

LIST OF TABLES

Table **page**

LIST OF FIGURES

ABBREVIATIONS, ACRONYMS AND SYMBOLS

A & B	Constants
B	Buildup factor
BEM	Boundary Element Methods
β	Propagation constant
c	Phase velocity of the ring mode
$c_{\circ}$	Vacuum speed of light
d	Thickness of the waveguide
DWDM	Dense wavelength division multiplexing
E	Electric field
E	Complex mode amplitudes
$E(t)$	Amplitude of a travelling wave
E_{i1}	Complex mode amplitude in the input waveguide one
E_{i2}	Complex mode amplitude in the input waveguide two
E_{t1}	Complex mode amplitude transmitted at throughput port
E_{t2}	Complex mode amplitude transmitted at drop port
$E_{t2-\mathrm{Re}sonance}$	Complex mode amplitude at drop port at resonance

e	Energy excited in the ring
F	Finesse of the ring
FDTD	Finite Difference Time Domain
FEM	Finite Element Methods
FSR	Free Spectral Range
FWHM	Full width half maximum
H	Magnetic field
HDF	Hierarchical Data Format
J & Y	Bessel functions
K	Number of layers
k	Power coupler coefficient
k	Vacuum wavenumber
k^* & t^*	conjugate of coupler parameter k and t
L	Circumference of the ring
M	Mode of the cavity
m	An integer
MEEP	MIT Electromagnetic Equation Propagation
MMI	Multimode interference

MPB	MIT Photonic Bands
n	Refractive index of material
n_c	Refractive index of the background
n_{eff}	Effective refractive index
n_g	Group refractive index
n_r	Refractive index of the ring
PMD	Polarization mode Dispersion
PML	Perfect Matched Layers
$P(t)$	Total power flowing through any cross section of the ring
P_{i2}	Power circulating in the ring
P_{t1}	Transmission power in the output waveguide
$P_{t2-\mathrm{Re}sonance}$	Resonance output power at the drop port
Q	Quality factor
Re	Real parts of the azimuthal indices
r	Radius of the ring
TE	Transverse Electric
TM	Transverse Magnetic

t	Power through coefficient
t	Time
τ	Decay time-constant
τ_{ie}	Decay time-constant in the power lost due to intrinsic effects
τ_{tr}	Decay time-constant in the transmitted wave
τ_{t2}	Decay time-constant in the power coupled to the output
	wavelength
v'	The real part of azimuthal number
v_g	Group velocity
WG	Waveguide
WDM	Wavelength Division Multiplexing
λ	Wavelength
ω	Angular frequency
λ_A	Wavelength in the add port
ω_R	Resonant frequency
λ_{res}	Wavelength at resonance
$\lambda_1, \lambda_2, \lambda_3$	Wavelength in the input port

$\Delta\lambda$	Difference between the vacuum wavelengths corresponding to two resonant conditions
α	Loss coefficient of the ring
φ_t	Phase of the coupler

CHAPTER ONE

INTRODUCTION

1.1 Background

It is almost impossible to imagine a world without long distance communication which means there will be no internet, no telephone, no radio or television. The first time an electronic message was sent over a long distance was in 1844 (Kominato, Ohmori, Takato, Okazaki and Yasu, 1992 and Franchimon, 2010). This led to the establishment of telegraphy. Years later, in 1876 Alexander Graham Bell found a way to transmit speech over long distances (Franchimon, Hiremath, Stoffer and Hammer, 2013) which resulted in the establishment of the first telephone company two years later. Since 1978 the number of telephone calls grew rapidly, and in about the midway of the twentieth century it became apparent that the demand for communication capacity would be too large and hence exceed the available facilities. A new way of transmitting signal was imperative and several solutions were suggested, but comparison of several options favored the use of optical fibres as the most feasible (Gambling, 2000).

The electromagnetic waves guides were treated by Lord Rayleigh (Okamoto, 2010) nearly 37 years after constitution of the Maxwell's equations (Griffiths and Reed 1999) for a nonmetallic circular cylindrical dielectric waveguide, what is now called a fibre. Fibre optics, though used extensively today, is a fairly simple and old technology. It is responsible for many modern revolutions in science and technology. This has been brought about primarily by the invention of the laser in 1960 (Thyagarajan and Ghatak, 2007). One of the most interesting applications of lasers is

in communication and computer networking. Use of electromagnetic waves in communication is quite old, but the invention of the laser ushered in a new source of high frequency electromagnetic wave as compared to microwaves and radio frequencies for use in communication systems. The development of low-loss optical fibers led to an explosion in the application of laser communication, and today we are able to communicate almost instantaneously between any two points on the globe (Thyagarajan and Ghatak, 2007). The fibre optics operates on the principle of total internal reflection or a light guide and was first demonstrated by (Hartig and Swanson, 1938)

The optical fibre has several advantages as compared to the electrical cables (Anderson, 1979) and among them are:

i. Broadband hence have a large carrying capacity of information.
ii. Immunity to Electromagnetic interference, hence are unaffected by electromagnetic radiation around it.
iii. Low attenuation loss over long distance, hence transmit signals over long distances with minimal boosting.
iv. Electrical insulator, are made from glass which is nonconductor of electricity hence no ground loops and leakages.
v. Low maintenance cost though installation cost is high.

Despite the success of fibre optics, their use is not commensurate to the increasing demand due to the ever growing number of the internet users and expansion of long distance communication (Kogelnik, 1975 and Nawrocka, Liu, Wang and Panepucci, 2006). This calls for more research on optical aspects to improve on the performance of optical fibre as means of communication. One of the ways to improve is by introduction of Resonators. A resonator is an arrangement of optical components,

which allows a beam of light to circulate in a closed path leading to a filter behavior. Such resonators can be made in different forms. These resonators include Ring resonators, waveguide resonators and Bulk-optical Resonators (Siegman, 1986, Magni, 1987, Hodgson and Weber, 2005 and Lalanne, Sauvan and Hugonin, 2008).

Bandpass filter based on ring resonator is a key component in modern Dense wavelength division multiplexing (DWDM) system applications (Little, Chu, Haus, Foresi and Laine, 1997, Chin and Ho, 1998 and Delâge, Xu, McKinnon, Post, Waldron, Lapointe and Schmid, 2009) for the implementation of the fundamental functions, such as channel add-drop, channel selection, demultiplexing and multichannel filtering (Kominato *et al*., 1992, Suzuki, Oda and Hibino, 1995, Little,Foresi, Steinmeyer, Thoen, Chu, Haus and Greene, 1998 Mansoor, Sasse, Al Asadi, Ison and Duffy, 2014). Some of these functions apply to a single channel of system, whereas others apply to a subset of channels (Tabib-Azar, and Beheim, 1997). The required characteristics of those functions are high stopband rejection in order to guarantee a low cross-talk between channels, a flat-top filter response, and low insertion loss (Zhang and Xue, 2007 and Elshoff and Rautenberg, 2010).

Most common method used to simulate the ring resonator is the finite-difference time-domain (FDTD) (Ediss, 2003 and Akleman, and Sevgı, 2008) and therefore MIT Electromagnet Equation Propagation (MEEP) software is an improved FDTD code developed by MIT photonics group. The MEEP software allows modeling, simulating and interpreting the physical factors affecting the ring resonators within a short computation time and it also occupies less memory compared to FDTD (Photonics, 2003).

The ring resonator is determined by the microwave substrate properties in particular the dielectric constant (Zhang and Xue, 2007). Normally, radiation losses are neglected when designing ring resonators to determine substrate parameter that are used in script for modeling it (Kaminow, Li and Willner, 2013). Experiments have been carried out on materials with known properties to test the validity of the theory and good agreement has been obtained (Hopkins, 2006).

Solutions for the modal wave propagation were first obtained in 1910 by Hondros and Debye (Prkna, Čtyroký, and Hubálek, 2004). However the early researchers were mostly interested in longer wavelengths, such as the propagation of microwaves in dielectric wires and dielectric rod antennas. Some of the examples were the experiments conducted in 1936 by the microwave waveguide at Bell Labs in Holmdel (Dadashi, Kurt, Üstün and Esen 2014); the predecessor of the current Crawford Hill Labs. In 1940s, the classical textbooks on electromagnetic wave propagation by Stratton and Schelkunoff contained chapters discussing the detailed solutions for the propagating modes of circular dielectric guides as well as metallic waveguides in terms of Bessel and Hankel functions (Emerson, 1997 and Schmidt and Russell, 2008). Among the papers they cited was the 1938 publication by Brillouin on the same subject (Chu and Barrow, 1938). The model solutions were of very general validity (Khalaj-Amirhosseini, 2006 and Stratton, 2007) allowing the specification of dielectric constant and finite conductivities (or laser gain) in both core and cladding. These solutions contained special cases both in the lossless dielectric guides for zero conductivity, and the hollow metallic waveguides of microwave technology for a lossless core and a cladding of finite conductivity (Hartig and Swanson, 1938 and Ksendzov, 2005). The hollow metal waveguides received a great deal of early

attention for microwave application such as RADAR and microwave radio transmission (Doerr and Kogelnik, 2008). Dielectric waveguides for optical applications received attention in the late 1950s (Griffel, 2000). These optical fibres were mostly contemplated for the imaging tasks and fiber optic face plates (Bates, 2001).

1.2 Problem statement

The computing industry has been steadily increasing the number of cores on a single processor to raise performance through computation. In order for multiprocessor systems to properly function and take advantage of the cores ring resonators filters are key in providing a large-bandwidth in nano scale on both on-chip (eg core to core) and off-chip (eg core to main memory) communication links for WDM. Ring resonator filters are also small in size and take advantage of high refractive indices. Electronic interconnection networks have thus far been capable of coping with communication demands of today's applications. However because of the high demand in large-bandwidth communications there is need to improve on data selection in the nano scale.

1.3 Justification

With an increasing demand for broadband access to internet and communication, there is need to check on the selection (filter) of the optical signals and data transmitted along a waveguide at any given time. Optical filters, Tunable filters, broadband switches and optical modulators can be developed out of ring resonators. Filters are useful in selectively extracting a subset of wavelengths from a WDM messages, Broadband Switches from the Ring resonators are also capable of controlling the flow of an entire WDM message by aligning each wavelength channel

to a mode of the ring, a modulator array can be formed with multiple ring modulators so that several wavelength channels can be encoded in parallel, creating a WDM signal. This will improve broadband access to internet and communication towards Fibre to the home (FTTH) hence fulfilling, one of the goals of vision 2030.

1.4 Objectives

The general objective of the thesis is to model and simulate a Ring resonator in MEEP with special characteristics as an optical Filter.

The specific objectives are:

1. To determine the resonant modes of a Ring resonator; resonant frequency and resonant wavelength.
2. To determine factors that affect the working of the Ring resonator.
3. To model a tunable filter based on a ring resonator.

CHAPTER TWO

THEORY AND LITERATURE REVIEW

2.1 Introduction

In this chapter the theory of the fields of the Ring resonator and the literature review of the Ring resonator are discussed.

2.2 Literature of Ring resonator

In 1961 Snitzer and Osterberg observed the mode patterns of fibres in the visible .The advent of the laser, together with the subsequent demonstration of low-loss fibres, laid the groundwork for optical fibre communication that has caused a revolution in the telecom industry (Yee, 1966). This created an urgent need and interest in the thorough and detailed understanding of light wave propagation in the circular guides of transmission fibres, the planar film and rectangular guides of semiconductor laser, optical integrated circuitry, and guided-wave optoelectronics (Ramaswami, 2002).

In 1969, Marcatilli proposed a ring or disk resonator which comprised of a ring and two straight waveguides. The two straight waveguides are known as the bus or the port waveguides, they are coupled to the ring with radius *r* by directional couplers through the evanescent field or by multimode interference (MMI) this was described on (Sobol, 1984 and Yariv, 2002).

The size of Ring resonators allows high density integration in optical photonic circuits due to the use of high index contrast. Ring resonators based Wavelength Division Multiplexing (WDM) is considered as an example in this technology (Mansoor *et al*., 2014).

One key importance of a Ring resonator is in the obtaining of resonant wavelength and the resonant frequency, these are values that determine whether a resonator will be in resonance or not and thus behaving as a filter this is as shown in Table 2.1 and Table 2.2

Table 2.1: The results of calculation using bent waveguide approach and complex frequency approach with resonance wavelength approximately 1.300 μm (Hiremath *et al.*, 2005).

Radius R [μm]	Ring microresonator					Disk microresonator, complex Frequency approach		
	Bent waveguide approach (λ=1.3 μm)			Complex freq approach				
	F	Re{v}	λ_{res} [μm]	F	v	λ_{res} [μm]	F	v
200	1.02×10^7	1605.106	1.30008	1.04×10^7	1605	1.30024	2.66×10^7	1612
100	520.67	802.779	1.29965	535.96	803	1.30082	1.64×10^5	811
80	81.22	642.368	1.30074	82.50	642	1.30094	4643.796	648
60	14.10	482.022	1.30006	14.41	482	1.30184	162.94	485
50	6.25	401.891	1.29965	6.40	402	1.30147	35.13	404
40	2.93	321.795	1.29919	3.00	322	1.30158	8.69	323
30	1.45	241.735	1.29859	1.49	242	1.29765	2.63	243
20	0.76	161.706	1.29763	0.78	162	1.29984	0.96	162
10	0.41	81.716	1.29513	0.42	82	1.29547	0.44	82
5	0.31	41.808	1.29192	0.32	42	1.29190	0.32	42

After a while (Hiremath *et al.*, 2005) similar work was done in the modeling circular optical micro resonators using whispering gallery modes and the results were compared with the ones in (Chaichuay, Yupapin and Saeung, 2009 and Franchimon, 2010), these were the resonant frequency which determine whether the Ring Resonator will be in resonance or not, to be in resonance then the resonant frequency should be in the range of 1.45 pHz as shown in Table 2.2

Table 2.2: The results for the ring with varying radius, whispering gallery modes with Eigen frequencies around 1.45 pHz

		Frequency from (pHz) (Chaichuay *et al*., 2009)		Calculated frequency (pHz) (Franchimon, 2010)	
$R_C(\mu m)$	m	$Re(\omega)$	$Im(\omega)$	$Re(\omega)$	$Im(\omega)$
5	42	1.4590	-5.428×10^{-2}	1.4559	-5.319×10^{-2}
10	82	1.4554	-2.113×10^{-2}	1.4544	-2.011×10^{-2}
20	162	1.4526	-5.748×10^{-3}	1.4508	-5.563×10^{-3}
30	242	1.4515	-2.013×10^{-3}	1.4520	-2.218×10^{-3}
40	322	1.4509	-7.507×10^{-3}	1.4510	-8.326×10^{-4}
50	402	1.4504	-2.819×10^{-4}	1.4500	-3.044×10^{-4}
60	482	1.4499	-1.044×10^{-4}	1.4500	-1.228×10^{-4}
80	642	1.4491	-1.368×10^{-5}	1.4490	-1.631×10^{-5}
100	813	1.4504	-1.685×10^{-6}	1.4500	-2.002×10^{-6}
200	1605	1.4499	-4.343×10^{-11}	1.4500	-7.707×10^{-11}

2.3 THEORY

The theory governing the operation and characteristics of a ring resonator, and its fabrication is discussed in this section.

2.3.1 Theory of Ring Resonator as a filter.

Ring resonators are key components in modern optical networks. Their size allows high density integration (Elosúa, Bariáin, Matías, Arregui, Luquin, Vergara, and Laguna, 2008). Micro-waveguide and fibre-based ring resonators are of great interest due to their versatile functionalities and compactness. They are being designed for different applications such as wavelength filtering, multiplexing, whispering gallery

mode switches, modulation, biosensing (Mansoor *et al*., 2014). Their main design characteristics are the circumference of the rings and the coupling ratios of the couplers that they include. The theory, design, fabrication and applications of micro resonators based on circular ring channel waveguides with lateral or vertical coupling to a signal input/output bus have been the subject of intense research (Little *et al*., 1997, Chin *et al*., 1998, Little, Chu, Pan and Kokubun, 2000 and Yariv, 2000). The layout of the channel dropping filter which was proposed is shown in

Fig.2.1.This can be regarded as the standard configuration for an integrated ring resonator channel dropping filter. A simpler configuration was obtained, when the second bus or port waveguide was removed as shown in Fig 2.2. Then the filter is typically referred to as “notch” filter because of the unique filter characteristic (Xu, Fattal and Beausoleil, 2008). The ring resonator simulation model is described beginning with the basic notch configuration and adding more bus waveguides and ring resonators to eventually build a multiple coupled ring resonator filter (Rabus, 2007).

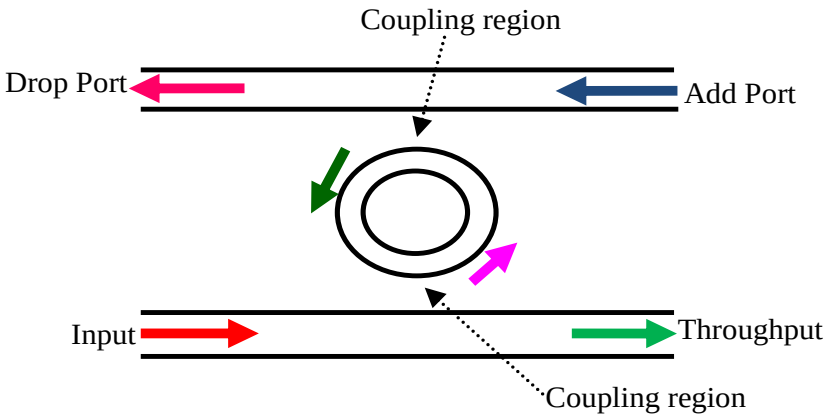

Figure 2.1: Ring resonator channel dropping filter.

2.3.2 Single Ring Resonators Basic Configuration

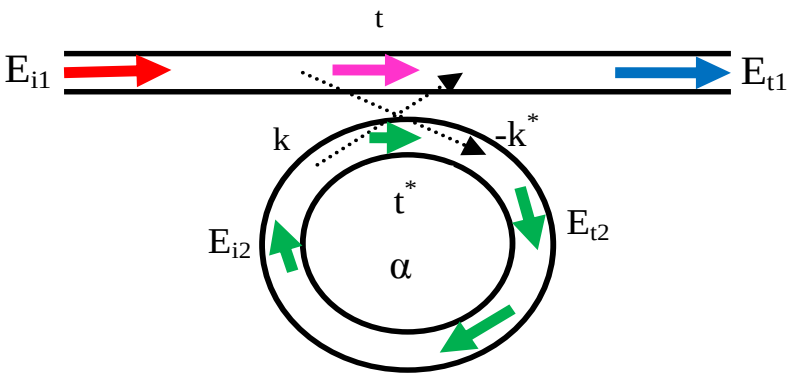

Figure 2.2: Model of a single ring resonator with one waveguide.

For single unidirectional mode of the resonator the losses occurring along the transmission of light in the waveguide and in the ring are incorporated in the attenuation constant whose interaction can be described by the matrix relation (Yariv 2000):

$$\begin{pmatrix} E_{t1} \\ E_{t2} \end{pmatrix} = \begin{pmatrix} t & k \\ -k^* & t^* \end{pmatrix} \begin{pmatrix} E_{i1} \\ E_{i2} \end{pmatrix} \tag{2.1}$$

The matrix represents a wave of (power-normalized) amplitude E_{i1} incident upon the coupling region and exits as E_{t1}, so that their squared magnitude corresponds to the modal power. The coupler parameters t and k is the diagonal element of the coupling matrix relating the input and output fields at the coupling element depends on the specific coupling mechanism used (Choi, Lee and Yariv 2001). The conjugate complex values of t and k are denoted by * respectively, they are the coupling parameters in the second straight guide.

The matrix is symmetric because the networks under consideration are reciprocal which in the lossless case obeys:

$$|k^2| + |t^2| = 1 \tag{2.2}$$

For further simplification of the modal, E_{i1} is chosen to be unity otherwise it can assume other values. Then the circulation trip in the ring is given by (Yariv, 2000);

$$E_{i2} = \alpha . e^{j\theta} E_{t2} \tag{2.3}$$

where α is the circulation loss factor of the ring and $\theta = \frac{\omega L}{c}$, L is the circumference of the ring, given by $L=2\pi r$, r being the radius of the ring measured from the center of the ring to the center of the waveguide, c is the phase velocity of the ring mode. $c = {}^{c_0}/_{n_{eff}}$ and ω is the fixed angular frequency $\omega=kc_0$, c_0 refers to speed of light in the vacuum . The vacuum wavenumber k is related to the wavenumber λ through: $k = {}^{2\pi}/_{\lambda}$. Using the vacuum wavenumber, the effective refractive index n_{eff} can be introduced into the ring coupling relation by (Zhang and Satpathy, 1990 and Agrawal, 2007);

$$\beta = k . n_{eff} = \frac{2\pi . n_{eff}}{\lambda} \tag{2.4}$$

β, is the propagation constant. Substituting L, k and c in θ in gives;

$$\theta = \frac{\omega L}{c} = \frac{k c_0 L}{c} = \frac{2\pi . n_{eff} . 2\pi r}{\lambda} = 4\pi^2 n_{eff} \frac{r}{\lambda} \tag{2.5}$$

Substituting for E in equation (2.1) to equation (2.3), the following equations are obtained (Choi *et al*., 2001).

$$E_{t1} = \frac{-\alpha + t.e^{-j\theta}}{-\alpha t^* + e^{-j\theta}} \tag{2.6}$$

$$E_{i2} = \frac{-\alpha k^*}{-\alpha t^* + e^{-j\theta}} \tag{2.7}$$

$$E_{t2} = \frac{-k^*}{1 - \alpha t^* e^{j\theta}} \tag{2.8}$$

The power transfer characteristics $\left|\frac{E_{t1}}{E_{i1}}\right|^2$ of the configuration are described by;

$$P_{t1} = \left|\frac{E_{t1}}{E_{i1}}\right|^2 = |E_{t1}|^2 = \frac{(\alpha - |t|)^2}{(1 - \alpha|t|)^2} \tag{2.9}$$

The modal, E_{i1} is chosen to be unity

where $t = |t|e^{j\varphi t}$, $|t|$ represents the coupling losses and φ_t the phase of the coupler.

The circulating power P_{i2} is given by (Yariv, 2000);

$$P_{i2} = |E_{i2}|^2 = \frac{\alpha^2(1 - |t|^2)}{1 - \alpha^2|t|^2 - 2\alpha|t|cos(\theta + \varphi_t)} \tag{2.10}$$

At resonance, $(\theta + \varphi_t) = 2\pi m$, where m is an integer, thus the equations of transmitted power and circulating power are obtained as follows:

$$P_{t1} = \left|\frac{E_{t1}}{E_{i1}}\right|^2 = |E_{t1}|^2 = \frac{(\alpha - |t|)^2}{(1 - \alpha|t|)^2} \tag{2.11}$$

$$P_{i2} = |E_{i2}|^2 = \frac{\alpha^2(1 - |t|^2)}{(1 - \alpha|t|)^2} \tag{2.12}$$

Two features of equation (2.11) illustrate most of potential applications;

1. There exists a special condition, $\alpha = |t|$ when the internal losses (1-α^2) are equal to the coupling losses $(1 - |t|^2)$ for which the transmitted power is zero, as shown in Fig. 2.3.

2. At $\alpha > |t|$ the transmission is much higher. It is apparent that in high-Q resonators, $\alpha \approx 1$, modulation in α for a given t or vice versa can control the transmitted power between unity and zero. This can be used to construct electro-optic modulators in switching technology. In addition to the under-coupled region $\alpha < |t|$, as the gain is increased, the power transmission decreases until the critical coupling point ($\alpha = |t|$) (Yariv, 2002).

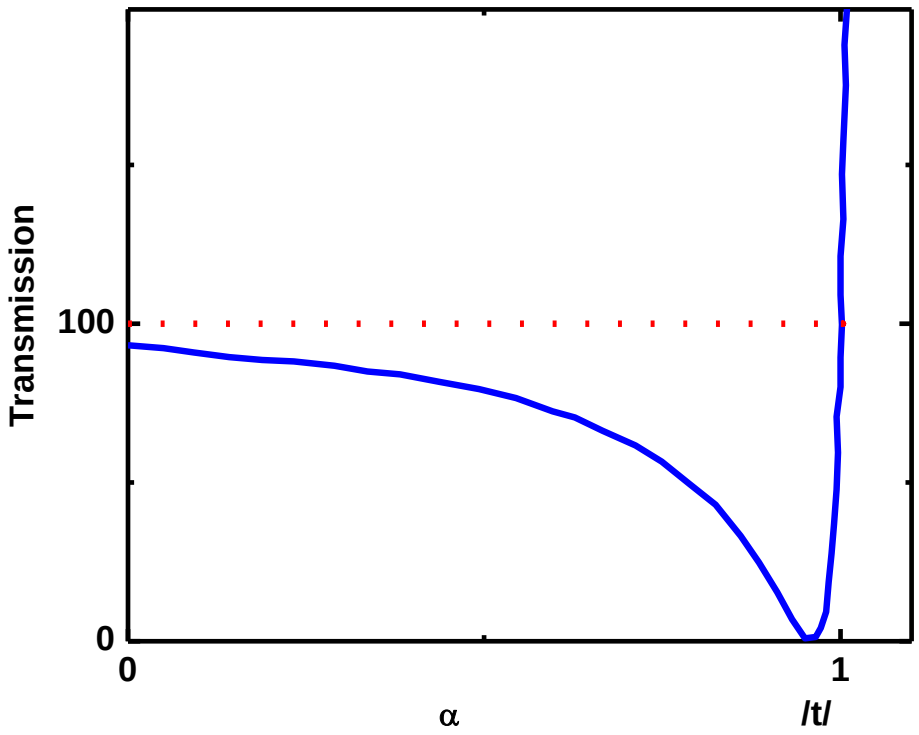

Figure 2.3: Critical coupling due to destructive interference (Choi *et al*., 2001)

From equation (2.11) and (2.12), it is possible to get a good idea of the behavior of a simplified basic ring resonator filter configuration consisting of only one waveguide

and a ring. The model above can be extended to suit the requirement of various types of ring resonator configurations.

The other configuration is the basic ring resonator add-drop configuration consisting of two straight waveguides comprising of four ports; input port, throughput port, drop port and add port as shown in Figure 2.4.

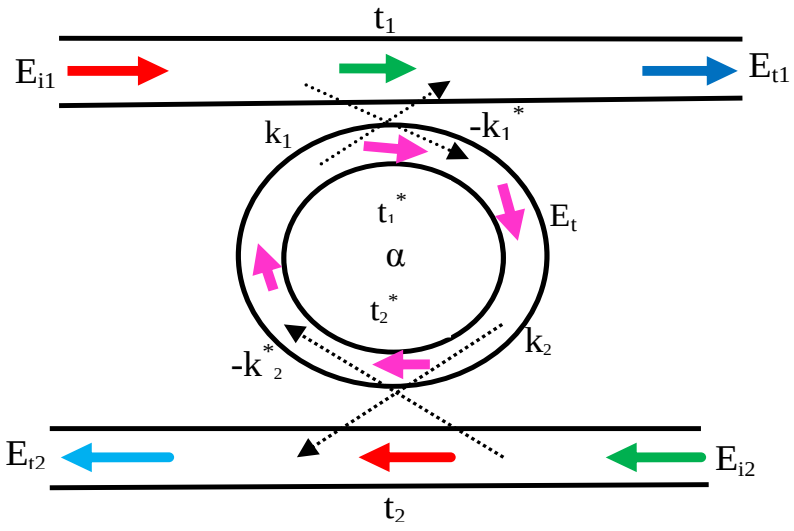

Figure 2.4: A basic add-drop single ring resonator filter.

The ring resonator simulation model just like the notch in Figure 2.2 E_{i1} is equal to 1 for simplification. The throughput mode amplitude E_{t1} in the first waveguide is given by (Yariv, 2000);

$$E_{t1} = t_1 + \frac{-k_1 k_1^* t_2^* \alpha_{1/2}^2 e^{j\theta |t_1|^2 + |k_1|^2 = 1}}{1 - t_1^* t_2^* \alpha_{1/2}^2 e^{j\theta}}$$

$$= \frac{t_1 - t_2^* \alpha_{1/2}^2 e^{j\theta}}{1 - t_1^* t_2^* \alpha_{1/2}^2 e^{j\theta}} = \frac{t_1 - t_2^* \alpha e^{j\theta}}{1 - t_1^* t_2^* \alpha e^{j\theta}} \qquad (2.13)$$

where ,$\alpha_{1/2}$ is the half round trip loss.

$$\alpha = \alpha_{1/2}^{2} \tag{2.14}$$

The mode amplitude in the ring has to pass the second coupler (see Figure 2.4) to become the new dropped mode amplitude E_{t2} (see Figure 2.5), and is given by;

$$E_{t2} = \frac{-k_1^* k_2 \alpha_{1/2} e^{j\theta_{1/2}}}{1 - t_1^* t_2^* \alpha e^{j\theta}} \tag{2.15}$$

where $\theta_{1/2}$ is the half round trip phase and $\theta = 2\theta_{1/2}$

A plot of the dropped power, E_{t2} against wavelength is shown in Figure 2.5

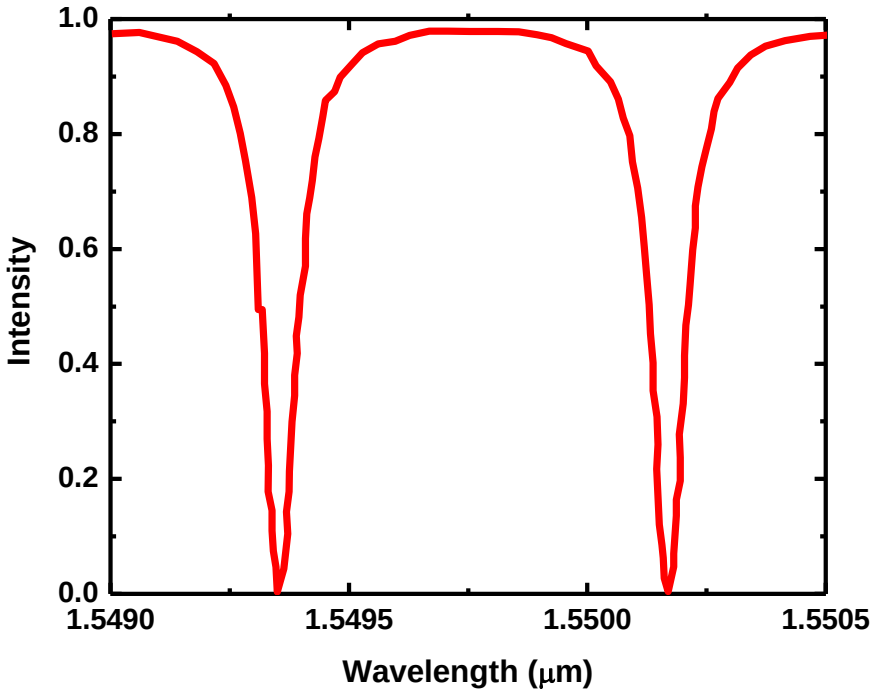

Figure 2.5: Notch type ring resonator filter characteristics –dropped power (Hiremath *et al.*,2005)

At resonance, the output power from the drop port is given by

$$P_{t2-Resonance} = |E_{t2-Resonance}|^2$$

$$P_{t2-Resonance} = \frac{(1-|t_1|)^2.(1-|t_2|^2).\alpha}{(1-\alpha|t_1 t_2|)^2} \quad (2.16)$$

If α = 1 the throughput port mode amplitude E_{t1} in equation (2.13) will be zero at resonance for identical symmetrical couplers $t_1 = t_2$, which indicates that the wavelength at resonance is fully extracted by the resonator. The value α = 1 can only be achieved by the implementation of gain incorporated in the ring resonator to compensate the waveguide losses. The loss coefficient α is fixed in a purely passing ring resonator. The possibility of achieving minimum intensity $P_{t1}=0$ at resonance is to adjust the coupling parameters t_1 and t_2 to the loss coefficient α such that

$$\alpha = \left|\frac{t_1}{t_2}\right| \quad (2.17)$$

If the ring resonator is lossless α = 1, then the coupler have to be symmetric

($t_1 = t_2$) in order to achieve minimum intensity. Transmissions of lossless ring resonator add drop filter is shown in Figure 2.6.

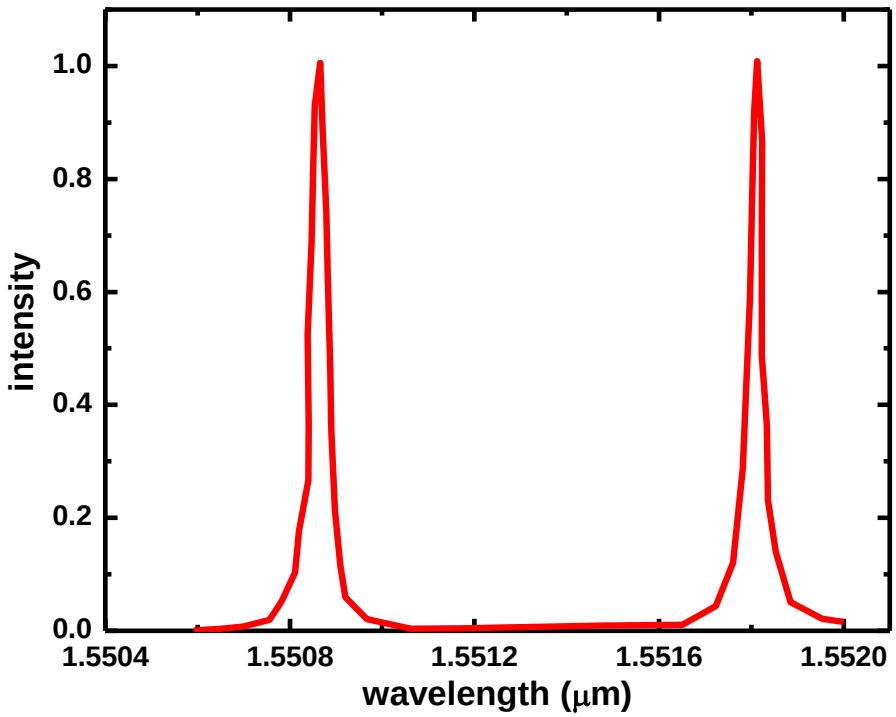

Figure 2.6: Add- port power ring resonator filter characteristic (Hiremath *et al*., 2005)

There are different kinds of requirements on the simulation of various ring resonator configurations. The ring model can be divided into more segments to account for different materials or modified waveguide paths.

2.4 Ring Resonator Parameters

The terms associated with ring resonators are defined in this section, they include; Free spectral range, Resonance width, Finesse of the ring and quality factor.

2.4.1 Free Spectral Range (FSR)

Optical resonators provide transmission spectra that are periodic in the frequency domain and they demonstrate narrow peaks followed by broad low power transmission (Elosúa *et al*., 2008). There is need therefore to measure the frequency interval between the peaks. FSR is the difference in position between two consecutive resonant peaks and can be defined either in frequency or wavelength domain (FSR_f or FSR_λ respectively)

$$FSR_f = \Delta f = \frac{c}{n_g 2\pi R}\ , FSR_\lambda = \Delta\lambda \approx \frac{\lambda^2}{n_g 2\pi R} \tag{2.18}$$

R is the radius of the ring, *c* the speed of light in vacuum, n_g is the group refractive index and Δf, $\Delta\lambda$ is the difference in position between two consecutive resonant peaks frequency and wavelength respectively (Rabiei, Steier, Zhang and Dalton, 2002).

2.4.2 Resonance Width

Resonance width is the full width at half maximum (FWHM) or 3dB bandwidth $2\partial\lambda$ of the resonance line shape. Using the equations 2.14 and 2.15 (Rabus, 2007).

$$\left|\frac{-k_1^* k_2 \alpha_{1/2} e^{j\theta_{1/2}}}{1 - t_1^* t_2^* \alpha e^{j\theta}}\right|^2 = \frac{1}{2}\,\frac{|k_1|^2|k_2|^2\alpha}{(1-\alpha|t_1 t_2|)^2} \tag{2.19}$$

Assuming that the coupling coefficients are real, lossless, and without a phase term, equation (2.22) can be written as (Yariv, 1973 and Rabiei *et al*., 2002)

$$\frac{k_1 k_2 \alpha_{1/2}}{1 - 2t_1 t_2 \alpha\cos(\theta) + (t_1 t_2 \alpha)^2} = \frac{1}{2}\,\frac{(k_1 k_2 \alpha_{1/2})^2}{(1 - t_1 t_2 \alpha)^2} \tag{2.20}$$

Then

$$2(1 - t_1 t_2 \alpha)^2 = 1 - 2t_1 t_2 \alpha cos(\theta) + (t_1 t_2 \alpha)^2 \tag{2.21}$$

For small θ, using the real part of the series expansion of the Euler formula

$$cos(\theta) = 1 - \frac{\theta^2}{2} \tag{2.22}$$

Therefore

$$\theta^2 = \frac{(1 - t_1 t_2 \alpha)^2}{t_1 t_2 \alpha} \tag{2.23}$$

This equation can further be simplified if the loss in the ring is negligible and the coupling is symmetric ($t = t_1 = t_2$) to

$$\theta = \sqrt{\frac{(1-t^2)^2}{t^2}} = \frac{1-t^2}{t} \tag{2.24}$$

This in full frequency width at half maximum (FWHM) will be (Yariv, 2000).

$$FWHM = \frac{2(1-|t|^2)c}{L} = \frac{2k^2c}{L} \tag{2.25}$$

where $\alpha = |t| \approx 1$

2.4.3 Finesse of the Ring, F

The finesse of an optical resonator is the free spectral range divided by the full width at half-maximum bandwidth of its resonances. It is fully determined by the resonator losses and is independent of the resonator length (Rabiei *et al*., 2002 and Elshoff and Rautenberg, 2010)

$$F = \frac{FSR}{FWHM} = \frac{\Delta\lambda}{2\delta\lambda} \tag{2.26}$$

2.4.4 Quality factor Q

It is the measure of the sharpness of the resonance parameter and is closely related to the finesse. It is defined as the ratio of the operation wavelength and the resonance width (Agrawal, 2001 and Rabiei *et al*., 2002).

$$Q = \frac{\lambda}{2\delta\lambda} = \pi \frac{n_{eff}L}{\lambda} \frac{t}{1-t^2} = \frac{n_{eff}L}{\lambda} F \tag{2.27}$$

The quality factor can be regarded as the stored energy divided by the power lost per optical cycle. The intensity in the ring resonator can be much higher than that in the bus waveguides, this is due to the traveling wave in the ring resonator interferes constructively at resonance with the input wave and thus the amplitude builds up. In addition to this intensity increase, the field also experiences a phase-shift of an integral multiple of 2π in one round trip. The intensity enhancement or buildup factor B is given by (Yarir, 1973).

$$B = \left|\frac{E_r}{E_{i1}}\right|^2 = \left|\frac{-k_1^*}{1 - t_1^* t_2^* \alpha e^{j\theta}}\right|^2 \tag{2.28}$$

On resonance, the intensity enhancement factor is

$$B = \left|\frac{-k_1^*}{1 - t_1^* t_2^* \alpha}\right|^2 \tag{2.29}$$

For a lossless resonator and setting $k = k_1 = k_2$ where $k << 1$, B can be written as (Yariv, 2000).

$$B = \frac{1}{k^2} \rightarrow \frac{F}{\pi} \tag{2.30}$$

$$\alpha = |t| \approx 1$$

This equation directly relates the intensity enhancement factor B to the finesse F. For all-pass filter configuration and on resonance, the buildup factor is given by

$$B = \frac{1 + t}{1 - t} \tag{2.31}$$

($t = t_1 = t_2$), since the coupling parameter for *t* is one.

The ring resonators can be used for nonlinear optical devices for example Optical parametric oscillators and amplifiers since the intensity in the resonator can be much higher than in the bus waveguide.

2.5 The Time-Dependent Relations

For the basic ring resonator add-drop configuration, it is assumed that the ring supports a traveling wave of amplitude *E(t)*, having total power *P(t)* flowing through any cross section of the ring waveguide at time *t*. The ring is regarded as an oscillator of energy *e(t)*, normalized so that *p(t)* is the total energy stored in the ring (Rabus, 2007). The relation between energy and power in the ring is given as;

$$P(t) = |e(t)|^2 = p(t)\frac{2\pi r}{v_g} \tag{2.32}$$

where v_g is the group velocity. The resonator has a resonant frequency of ω_R and amplitude decay time-constant of $1/\tau$. The decay rate is a function of the power exciting the ring resonator, which is expressed as a function of the power coupled to the transmitted wave $1/\tau_{tr}$, power lost due to intrinsic effects $1/\tau_{ie}$, and the power coupled to the output wavelength $1/\tau_{t2}$ (Rabus, 2007). That is:

$$1/\tau = 1/\tau_{tr} + 1/\tau_{ie} + 1/\tau_{t2} \tag{2.33}$$

The time rate of change in the ring energy can then be expressed as

$$\frac{d}{dt}e = \left(j\omega_R - 1/\tau\right)e^{-k^*}.E_{i1} \tag{2.34}$$

The relation between the coupling parameter *k* and the decay rates of the transmitted wave $1/\tau_{tr}$ and the output waveguide $1/\tau_{t2}$, is determined by the power conservation. When the ring resonator is excited to energy of $|e_0|^2$, no output wave is present and no input wave E_{i1} goes to E_{t1}.

The energy in the ring assuming no intrinsic loss will decay as follows;

$$|e(t)|^2 = |e_0|^2 \exp\left(\frac{-2t}{\tau_{tr}}\right) \tag{2.35}$$

The power transfer characteristic for the drop port can be calculated with the input wave E_{i1} being proportional to $exp(j\omega t)$ (Rabus, 2007).

$$e = \frac{-j\sqrt{\frac{2}{\tau_{tr}}}}{j(\omega - \omega_R) + \frac{1}{\tau}} E_{i1} \tag{2.36}$$

From equation (2.34), the transmitted wave at the throughput port can be determined as:

$$E_{t1} = E_{i1} - k^* e = \frac{j(\omega - \omega_R) + \frac{1}{\tau} + jk^*\sqrt{\frac{2}{\tau_{tr}}}}{j(\omega - \omega_R) + \frac{1}{\tau}} E_{i1} \tag{2.37}$$

Finally the drop port power transfer characteristic is obtained by using the equation for power conservation (when $E_{i2} = 0$):

$$|E_{t2}|^2 = |E_{i1}|^2 - |E_{t1}|^2 = \frac{2}{\tau_{t2}}|e|^2 = \frac{\frac{4}{\tau_{t2}\tau_{tr}}}{(\omega - \omega_R)^2 + \frac{1}{\tau}} |E_{i1}|^2 \tag{2.38}$$

Equation (2.38) can be simplified further if both waveguides couple equally to the ring ($\tau_{t2} = \tau_{tr}$) (Elshoff and Rautenberg, 2010).

2.6 The Maxwell equations

The first step is to look at the Maxwell equations which are given by (Kogelnik, 1975).

$$\nabla \times E = -\mu \frac{\partial H}{\partial t} \qquad (2.39a)$$

$$\nabla \times H = \varepsilon \frac{\partial E}{\partial t} \qquad (2.39b)$$

$$\nabla . H = 0 \qquad (2.39c)$$

$$\nabla . \varepsilon E = 0 \qquad (2.39d)$$

where E is the electric field, H the magnetic field, ε is the permittivity and μ is the permeability. The field and structure is assumed to be constant in the y-direction. All fields will be time harmonic and so the time dependence can be described by $e^{-i\omega t}$, where ω is the frequency which is a complex number (Oxborrow, 2007).

Reducing equations (2.39a) and (2.39b) by filling the time-derivative in Cartesian coordinates gives;

$$\begin{bmatrix} \frac{\partial E_z}{\partial y} & -\frac{\partial E_y}{\partial z} \\ \frac{\partial E_x}{\partial z} & -\frac{\partial E_z}{\partial x} \\ \frac{\partial E_y}{\partial x} & -\frac{\partial E_x}{\partial y} \end{bmatrix} = i\omega\mu_0 \begin{bmatrix} H_x \\ H_y \\ H_z \end{bmatrix} \qquad (2.40)$$

$$\begin{bmatrix} \frac{\partial H_z}{\partial y} & -\frac{\partial H_y}{\partial z} \\ \frac{\partial H_x}{\partial z} & -\frac{\partial H_z}{\partial x} \\ \frac{\partial H_y}{\partial x} & -\frac{\partial H_x}{\partial y} \end{bmatrix} = -i\omega\varepsilon \begin{bmatrix} E_x \\ E_y \\ E_z \end{bmatrix}$$

(2.41)

The solutions to the problems treated here are invariant in the *y*-direction because they are constant along *y*-direction. Therefore all *y*-derivatives will varnish. Equations (2.40) and (2.41) will split in two independent sets. The first involves E_y, H_x and H_z and the second E_x, E_z and H_y. These are associated with Transverse electric (TE) and Transverse magnetic (TM) polarization respectively. The equations are (Yee, 1966).

$$H_x = \frac{1}{-i\omega\mu_0}\frac{\partial E_y}{\partial z} \qquad (2.42a)$$

$$H_z = \frac{1}{i\omega\mu_0}\frac{\partial E_y}{\partial x} \qquad (2.42b)$$

$$-i\omega\varepsilon E_y = \frac{\partial H_x}{\partial z} - \frac{\partial H_z}{\partial x}$$

$$= \frac{-1}{i\omega\mu_0}\left(\frac{\partial^2 E_y}{\partial z^2} + \frac{\partial^2 E_y}{\partial x^2}\right) \qquad (2.42c)$$

When equation (2.42c) is rewritten, will be (Chew and Weedon, 1994)

$$0 = \left[\frac{\partial^2}{\partial x^2} + \frac{\partial^2}{\partial z^2} + \omega^2\mu_0\varepsilon\right]E_y \quad = \quad [\nabla^2 + \omega^2\mu_0\varepsilon]E_y \qquad (2.43)$$

Rewriting equation (2.43) with $\varepsilon = \varepsilon_0 \varepsilon_r$ where ε_0 is the permittivity of free space, and $\varepsilon_r = n^2$, n is the refractive index of the material, and expressing it in terms of the speed of light (Kogelnik, 1975),

$$c^2 = \frac{1}{\mu_0 \varepsilon_0} \quad , \qquad \left[\nabla^2 + \frac{\omega^2 n^2}{c^2}\right] E_y = 0 \tag{2.44}$$

2.7 Finite element

The finite elements are used in the z-direction and the aim is to determine the unknown amplitudes in equation (3.13). Quantities f_1, b_1, f_2 and b_2 are functions of z, hence they will be discretized. The computational window $[Z_0, Z_N]$ is divided into N pieces of length $\Delta z = (Z_N - Z_0)/N$. Nodal points are placed at $Z_j = Z_0 + j\Delta Z$, with j=0,…,N. For each node the piecewise linear function $\alpha_j(z)$ is given by (Chin and Ho, 1998).

$$\alpha_j(z) = \begin{cases} \left(z - z_{j-1}\right)/\Delta z, & if\ z_{j-1} \le z < z_j \\ \left(z_{j+1} - z\right)/\Delta z, & if\ z_j \le z < z_{j+1} \\ o \qquad\qquad , elsewhere \end{cases}$$

(2.45)

This has an exception that $\alpha_0 = 1$ for $z < z_0$ and $\alpha_N = 1$ for $z > z_n$

By use of these functions, a first order discretization of $f_1(z)$ into linear finite elements is given as:-

$$(z) = \sum_j f_j^1 \alpha_j(z) \tag{2.46}$$

The other amplitudes are discretized in the same way

All amplitudes f_j^1,b_j^1,$f_j^2$and b_j^2 are collected together with the unknowns γM in one set $\{a_k\}$. The total field from equation (2.40) will be:-

$$\begin{bmatrix} E \\ H \end{bmatrix}(x,z) = \sum_k a_k \begin{bmatrix} E_k \\ H_k \end{bmatrix}(x,z) \tag{2.47}$$

where E_k H_k are an assembly of $\alpha_j(z)\psi_{\mathrm{n}}^{\pm}(\mathrm{x},\mathrm{z})$ and $\psi_3^{\mathrm{M}}(\mathrm{x},\mathrm{z})$ respectively. From the frequency domain of the Maxwell equations (Chew and Weedon, 1994)

$$\nabla \times E - i\omega\mu_0 H = 0 \tag{2.48a}$$

$$-\nabla \times H - i\omega\varepsilon E = 0 \tag{2.48b}$$

To obtain equation (2.49, equation (2.48a) is multiplied with a complex conjugate (*) of a trial field H′ and equation (2.48b) with a complex conjugate of trial field E′, add them together and integrate the whole sum. The resulting equation will be (Oxborrow, 2007):-

$$\iint \{(H')^*.(\nabla \times E) - (\mathrm{E}')^*.(\nabla \times \mathrm{H}) - \mathrm{i}\omega\varepsilon(\mathrm{E}')^*.\mathrm{E} - \mathrm{i}\omega\mu_0(H')^*.H\}dxdz = 0 \tag{2.49}$$

The quality should hold for all trial fields E′ and H′

The fields in equation (2.48) can now be substituted for *E* and *H* in equation (2.49). If for the trial fields the modal elements E_l and H_l are used the resulting integral should vanish for every *l*. equation (2.49) then becomes (Yariv, 1973):

$$\sum_k k_{lk} a_k = 0 \tag{2.50}$$

for all *l*, where *l* is the length of the guide

$$K_{lk} = \iint\{(H_l)^*.(\nabla \times E_k) - (E_l)^*.(\nabla \times H_k) - \mathrm{i}\omega\varepsilon(E_l)^*.E_k - i\omega\mu_0(H_l)^*.H_k\}dxdz \qquad (2.51)$$

Since the input will only enter in the left side of waveguide1, f_0^1 should be equal to 1 and b_N^1,f_0^2 and b_N^2 should be zero. On substituting these constants for a_k in equation (2.52) and re-ordering entries results in a system given as:-, **g** are at the top, followed by the unknowns **u** and build a matrix K which consists of all those K_{lk} in the order in which they appear in **a**. this results in a system Ka

$$\begin{bmatrix} K_{gg} & K_{gu} \\ K_{ug} & K_{uu} \end{bmatrix} \begin{bmatrix} g \\ u \end{bmatrix} = 0 \qquad (2.52)$$

where g and u are normalized Bessel coefficients.

Since the 4 elements of g are already given, this system has more equations than unknowns and is over determined.

To handle this, the system will be solved in a least square sense, by rewriting equation (2.52) into

$$\begin{bmatrix} K_{gg} \\ K_{ug} \end{bmatrix} g = \begin{bmatrix} -K_{gu} \\ K_{uu} \end{bmatrix} u \qquad (2.53)$$

or

$$-K_g g = K_u u$$

The unknown coefficient in u can be found by solving

$$-K_u^{\sim} K_g g = K_u^{\sim} K_u u. \text{ Hence } u = -(K_u^{\sim} K_u)^{-1} K_u^{\sim} K_g g.$$

where ~ is the adjoint for matrix K.

This step translates the solution back to the electric and magnetic fields. This is done by substituting the coefficients in u and g into equation (2.52). However, even without this back translation, the coefficients in u give important information; the coefficients which belongs to the element related to the drop port that corresponds to the amplitude of the field at the left side of the waveguide 2, its square corresponds to the relative amount of dropped power P_D. If this number is large than P_T then the ring is in resonance and vice versa. In the same way the $P_{F,}$ P_T and P_R can be determined (Franchimon, 2010 and Franchimon *et al*., 2013).

2.8 Perfect matched layer (PML)

A perfectly matched layer (PML) is an artificial layer designed to obey Maxwell's equation with superior absorbing properties to those of a real material (Loh, Oskooi, Ibanescu, Skorobogatiy, 2009). A key property of a PML medium is that an electromagnet wave incident upon the PML from a non-PML medium does not reflect at the interface. Its use eliminates spurious reflections, a source of numerical problems in practice. The concept of PML was first developed by Berenger in 1994 (Berenger, 1994) and has gone several reformulations since then. Berenger employed a split form of Maxwell's equations, introducing additional terms for the electric field, but this form still matched Maxwell's equations exactly. However these additional electric fields cannot be associated with any physical fields. To circumvent this deficiency, two years later Gedney introduced a modified approach called unspilt PML (UPML) that makes use of physical fields (Gedney, 1996). Later, a novel way to construct PML was introduced by Zhao (Zhao and Cangellaris, 1996). This approach is called

generalized theory-based PML (GTPML) and makes use of a complex coordinate stretching in the frequency domain. More specifically, PMLs were shown to correspond to a coordinate transformation in which one (or more) coordinates are mapped to complex numbers. This transformation essentially constituted an analytic continuation of the equation into complex domain, replacing propagating waves with exponentially decaying waves.

CHAPTER THREE

METHODOLOGY

3.1 Introduction

This chapter presents the software, theoretical models, operating modes of the ring resonators studied for data generation and analysis. The model properties of both straight waveguides and circular ring are discussed. In its simplest version, a ring resonator includes a ring cavity and a coupling region. It starts with the Maxwell equations and describes how the specific step by step on how the electric field of a straight waveguide and the ring were determined.

3.2 MEEP software

MEEP is a free-difference time-domain (FDTD) simulation software package developed at MIT. Its features include simulation in 1-D, 2-D, 3-D, cylindrical coordinates and field analyses. A time-domain electromagnetic simulation takes Maxwell's equations and evolves them over time within some finite computational region. This can be used to calculate resonant modes and frequencies by analyzing the response of the system to a short pulse. The frequencies, decay rates and field patterns of the harmonic modes of a system including waveguides and cavity modes are extracted from MEEP.

The simulation is done in the structure exploring the fact that the system has continuous rotational symmetry by performing the simulation in cylindrical coordinates prepared in a control file.

In both models of the straight waveguide and a ring resonator, MEEP analyses the fields *f(t)* at any given point and expresses this as a sum of modes in the specified bandwidth.

$$f(t) = \sum_{n} a_n \, e^{-i\omega_n t} \tag{3.1}$$

where a_n is the complex amplitude and ω_n is the complex frequencies.

The quality factor (Q) is expressed as a ratio of the real part of ω_n to the imaginary part of ω_n(a negative imaginary part corresponds to an exponential decay)

$$Q = \frac{Re\omega}{-2Im\omega} \tag{3.2}$$

Q represents the number of optical periods for the energy to decay by expt(-2π) and $\frac{1}{Q}$ is the fractional bandwidth at half-maximum of the resonance peak (Meep).

3.3 The fundamental mode of a straight waveguide

Figure 3.1 shows a straight waveguide with no light transmitted. The electric field and solutions of a straight waveguide were determined, with a condition that the refractive indices below and above the wave guide boundary are equal.

Figure 3.1: A straight waveguide with no light transmitted.

The geometrical construction was done in cell whose size was 16 square units, the diameter of the waveguide was set to unity, PML layers were then introduced inside by coding, the refractive index was set at 3.4 and frequency source was placed to the left end of the waveguide. The transfer of the input was then observed throughout the waveguide by the running time set, the fields were then extracted from Hierarchical Data Format (HDF) a software in MEEP as shown in Figure 3.2.

The field in this case is assumed to propagate in the z-direction with propagation constant β, described by a z-dependence of $e^{i\beta z}$, for a given real frequency ω.

Substituting $e^{i\beta z}$ in equation (2.44) and $k = \frac{\omega}{c}$ as the wavenumber (Chew and Weedon, 1994) gives:

$$\left[\frac{\partial^2}{\partial x^2} - \beta^2 + k^2 n^2\right] E_y(x) = 0 \tag{3.3}$$

The total field will be in the form (Yee, 1996 and Chew and Weedon, 1994)

$$E(x, y, t) = E_y(x) e^{i(\beta z - \omega t)} \tag{3.4}$$

Figure 3.2 presents a model of a straight waveguide in MEEP that is transmitting power from a source current through some distance. In Figure 3.2 only the real part of the total field, including the time dependence shown at an arbitrary time, this is the physical part because the frequency value is positive. For positive β, in time this field moves in the positive z-direction. The field oscillates but does not decay in time since its propagating in one direction.

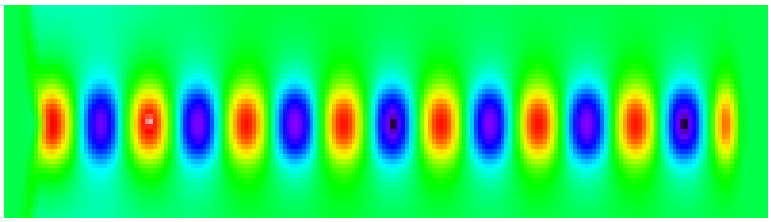

Figure 3.2: Light being transmitted in a straight waveguide.

3.4 The fundamental mode of a Ring

In this section the electric field of a ring is explained. The model can be used for structures with more layers. These layers are numbered in increasing order from the inner layer to the outer layers.

The geometrical construction was done in cell whose size was 16 units in the x-direction, 16 units in the z-direction and zero in the y-direction with ring thickness of 1 μm, PML layers were then introduced inside ,the refractive index was set at 3.4 and frequency source was placed at the lower part of the ring. The transfer of the input was then observed throughout the ring by the running time set, the fields were then extracted from HDF as shown in Figure 3.3.

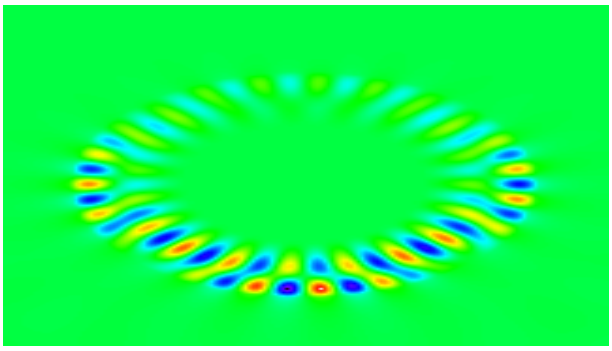

Figure 3 .3: The electric field of a ring.

In Figure 3.4 the search is for a resonant solution, where the field oscillates harmonically in time. The oscillation describes a time dependence of $e^{i\omega t}$, where ω is a complex number.

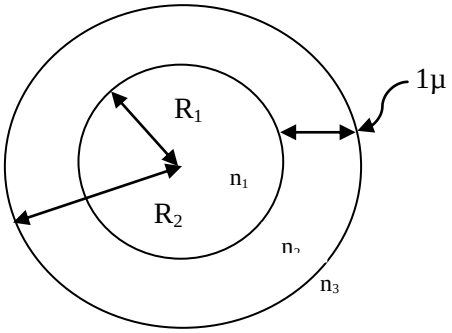

Figure 3.4: A model of a ring resonator. (Author, 2015)

The physical relevant solution should decay in time because the cavity is lossy, thus the imaginary part of ω should be negative, implying that the real part of $i\omega t$ will be positive, hence obtaining the decay time. The target frequency should be close to the real part of ω (Franchimon, 2010 and Melloni, Carniel, Costa and Martinelli, 2001).

$$Re(\omega) = 2\pi\, {}^{c}/_{\lambda} \tag{3.5}$$

where λ, is the target wavelength.

Cylindrical coordinates (*r, φ*) are chosen because of circular symmetry of the ring. The desired resonance is obtained when the fields is exactly equal to the original fields after making one round trip. This is an angular dependence $e^{im\varphi}$ of the electric field, where *m* is an integer.

Substituting *Re*(*ω*) in equation (3.5) to equation (3.3), the following equation is obtained (Chew and Weedon, 1994):

$$\left[\frac{\partial^2}{\partial r^2} + \frac{1}{r}\frac{\partial}{\partial r} + \frac{\omega^2 n^2}{c^2} - \frac{m^2}{r^2}\right] E_y(r) = 0 \tag{3.6}$$

By multiplying through by r^2 gives

$$\left[r^2\frac{\partial^2}{\partial r^2} + r\frac{\partial}{\partial r} + r^2\frac{\omega^2 n^2}{c^2} - m^2\right] E_y(r) = 0 \tag{3.7}$$

Equation 3.7 is Bessel equation, whose solutions are Bessel functions J and Y. These functions depend on the following boundary conditions which are chosen for each region:

i. At the origin the field should be finite

ii. At each interface the continuity conditions should hold, (both electric field and magnetic field which are tangential to the interface should be continuous). This condition implies that the r-derivative of E_y is continuous.

iii. In the outer layer the waves should be outgoing.

Note that the variable *m* appears in a quadratic manner in equation (3.7)

hence the solutions for $\pm m$ are identical. Positive *m* is chosen for the counter clockwise rotation.

In the layer which includes the origin the only possible solution is the Bessel function of the first kind, since this is the only Bessel function which is finite in the origin, as described by (Franchimon, 2010);

$$E_y(r) = a_1 J_m\left(\frac{\omega}{c} n_1 r\right) \tag{3.8}$$

n_1 is the refractive index of layer 1 and a_1 is the constant unknown for the moment.

In this case the electric field will be given by;

$$E_y(r) = a_{2k-2} - J_m\left(\frac{\omega}{c} n_k r\right) + a_{2k-1} Y_m\left(\frac{\omega}{c} n_k r\right) \tag{3.9}$$

The outer region requires that the waves should be outgoing for which the solution to this property for the time dependence will be the Hankel function of the first kind. The electric field in this case is described by

$$E_y(r) = a_{2k-2} H_m^{(1)}\left(\frac{\omega}{c} n_k r\right) \tag{3.10}$$

If $E_y(r)$ is known, the total field is determined by multiplying it with $e^{i(m\varphi-\omega t)}$. The general behavior of the field will be a field rotating in a counter clockwise direction since the field will be coming from the lower straight guide.

3.5 Coupling the waveguide and the Ring

The diagram in Figure 3.5 shows geometrical construction of two waveguides and a ring, which form a resonator as described below. The two waveguides and a ring are explained on how they form a resonator. The two straight waveguides have the same thickness *2d* and refractive index n_g. They are located at a distance *g* below and above the ring. The source is placed in the left side of the lower waveguide. Part of the incoming power P_T is transmitted to the right outlet of the waveguide 1, another part of the incoming power P_D will be transmitted to the left outlet of the upper waveguide 2. A small part P_R of the incoming power will be reflected to the left outlet of the waveguide 1 and a part P_F will be transmitted to the right outlet of waveguide 2 (Franchimon, 2010 and Griffel, 2000).

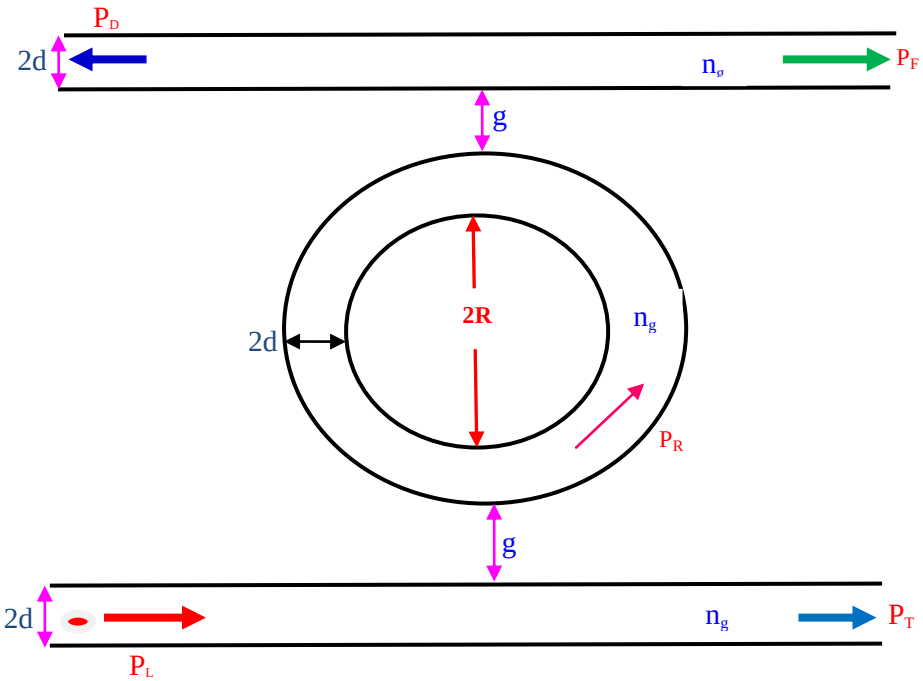

Figure 3.5: dimensions and power transmission of a single Ring Resonator.

The ring has a radius of R, with a thickness of 1 μm, refractive index of n_g and the background having a refractive index $n_c = 1$ (air).

If the electric field and magnetic fields are known, the fundamental mode of the waveguides is taken in to account. The fields of the waveguides are then of the form (Kokubun, Hatakeyama, Ogata, Suzuki and Zaize, 2005).

$$\psi_{\mathrm{n}}^{\pm}(\mathrm{x},\mathrm{z}) = \left[\begin{matrix}\widetilde{\mathrm{E}}\\ \widetilde{\mathrm{H}}\end{matrix}\right]_{\mathrm{n}}^{\pm}(\mathrm{x})\mathrm{e}^{\pm\beta\mathrm{z}} \qquad (3.11)$$

for n=1,2

The positive and negative sign indicate the modes propagating to the right and left respectively, *n* denotes the waveguide in which the field corresponding to $\tilde{E}$ and $\tilde{H}$ are the electric and magnetic part of the mode profile. For the ring the fields will be

$$\psi_3^M(x,z) = \left[\begin{matrix}\tilde{E}\\ \tilde{H}\end{matrix}\right]_M(x,z) \qquad (3.12)$$

where M is the mode of the cavity, which can either be a counter clockwise propagating mode with a positive angular wave-number *m* or a clockwise propagating mode with a negative angular wave-number.

The total field in the resonator consists of the fields in the waveguides and the ring (Oxborrow, 2007).

$$\left[\begin{matrix}E\\ H\end{matrix}\right](x,z) = f_1(z)\psi_1^+(x,z) + b_1(z)\psi_1^-(x,z) + f_2(z)\psi_2^+(x,z) + b_2(z)\psi_2^-(x,z) + \sum \gamma M \psi_3^M(x,z) \qquad (3.13)$$

where f_1, b_1, f_2, b_2 are modal amplitude in z-direction.

The components of the initial fields in the structure (waveguide or Ring) may not be disturbed by the presence of other components, except for functions f_1, b_1, f_2, b_2 and the coefficients γM (Franchimon, 2010).

CHAPTER FOUR

RESULTS AND DISCUSSION

4.1 Introduction

In this chapter, the results are presented. These include the resonant modes, the factors affecting the power transmission in a straight waveguide, the ring and the filter characteristics of a ring resonator and the shift in the resonator; a process of making a tunable filter.

4.2 Numerical Results

The numerical results obtained with the MEEP code written to solve for the resonant field of the ring are presented. Results obtained were compared to numerical results of whispering gallery modes (Hiremath, *et al* 2005).

The radius of the ring R_1 is the radius from the center of the ring, $R_2 = R_1 + 1$ μm, where 1μm was the thickness of the ring in Figure 4.1. The refractive index of the ring used was n=3.4 which was a high refractive index contrast to efficiently guide the light in the waveguide and ring (Snitzer and Osterberg, 1961). The parameters were determined by coding them in MEEP.

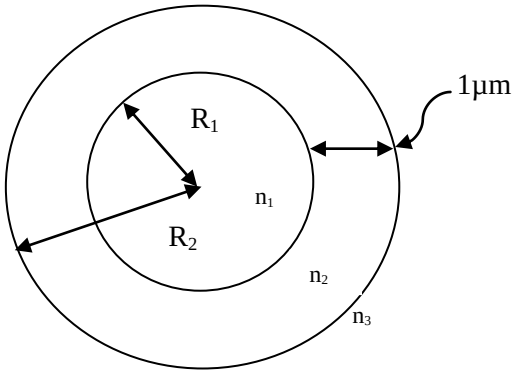

Figure 4.1: Ring with radii R_1, R_2 and refractive indices increasing from centre. (Author, 2015)

The tested structures had radii of between R_2 = 5 μm and R_2 =200 μm which were compared to (Franchimon, 2010). The integer representing the round trip for

resonance *m* was chosen equal to the value in theory for verification and improvement (Xiao, Min, Jiang, Dong and Yang, 2008).

Table 4.1 and 4.2 shows how the variation in the radius and *m* presented the real and imaginary resonant frequencies as well as the resonant wavelength of the ring.

The resonance wavelength that results in a real angular frequency of 1.45 x 10^{15} rad/s should be approximately λ=1.3 μm.

Table 4.1: Comparison of numerical and analytic results for varying radius having modes with frequencies approximately 1.45518 x 10^{15} rad/s

R_C (μm)	*M*	**Numerical** Frequency (x 10^{15} rad/s) **(MEEP)**		**Analytical** Frequency (x 10^{15} rad/s) (Franchimon ,2010)		**Deviation** **(Analytical – Numerical)**
		Re (ω)	**Im (ω)**	**Re (ω)**	**Im (ω)**	**Re (ω)**
5	42	1.4664	-5.9068 x 10^{-2}	1.4590	-5.428 x 10^{-2}	+0.0074
10	82	1.4753	-2.2411 x 10^{-2}	1.4554	-2.113 x 10^{-2}	+0.0199
20	162	1.4766	-1.5963 x 10^{-3}	1.4526	-5.748 x 10^{-3}	+0.024
30	243	1.4493	-0.0021 x 10^{-3}	1.4515	-2.013 x 10^{-3}	-0.0022
40	323	1.4531	-1.0918 x 10^{-4}	1.4509	-7.507 x 10^{-3}	+0.0022
50	404	1.4646	-1.7050 x 10^{-5}	1.4504	-2.819 x 10^{-4}	+0.0142
60	485	1.4343	-6.4681 x 10^{-5}	1.4499	-1.044 x 10^{-4}	-0.0156
80	648	1.4509	-3.9112 x 10^{-7}	1.4491	-1.368 x 10^{-5}	+0.0018
100	811	1.4327	-3.9771 x 10^{-8}	1.4504	-1.685 x 10^{-6}	-0.0177
200	1612	1.4486	-1.3384 x 10^{-13}	1.4499	-4.343 x 10^{-11}	-0.0013

For the resonant wavelength 1.2955μm was achieved. These resonant frequency and resonant wavelength are the modes that make a ring of any radii to be in resonance at any given point and thus become a Filter. This is as shown in Table 4.2.

Table 4.2: Ring with varying radius- having modes with wavelength approximately λ=1.2955 μm.

R_C (μm)	m	Numerical (MEEP)		Analytical (whispery gallery mode) (Franchimon ,2010)	Deviation
		Frequency (x 10^{15} rad/s)	Wavelength (μm)	Wavelength (μm)	Analytical – Numerical
5	42	1.4664	1.285	1.29192	-0.00692
10	82	1.4753	1.278	1.29513	-0.01713
20	162	1.4766	1.277	1.29763	-0.02063
30	243	1.4493	1.301	1.29859	+0.00241
40	323	1.4531	1.297	1.29919	-0.00219
50	404	1.4646	1.287	1.29965	-0.01265
60	485	1.4343	1.314	1.30006	+0.01394
80	648	1.4509	1.299	1.30074	-0.00174
100	811	1.4327	1.316	1.29965	+0.01635
200	1612	1.4486	1.301	1.30008	+0.00092

Since the results are in agreement with the literature, MEEP as an FDTD open source software can be used to simulate, model and calculate both the resonant frequency and resonant wavelength of a ring.

4.3 Straight waveguide

A straight waveguide is taken into consideration with parameters n=3.4 refractive index of the waveguide, w=1 μm width of the waveguide, pad=4 μm padding between the waveguide and the edge of PML, dpml=2 μm thickness of the PML, fcen=0.15 pHz pulse center frequency, df= 0.1 μm pulse width (in frequency). Computation cell 16 units in the x-direction, 8 units in the y-direction and zero units in the z-direction, it meant that the waveguide was in two dimensional and the computation time step of 200, this were the inputs coded in MEEP.

4.3.1 Variations in dielectric constant (ε)

The dielectric of the materials affects the fields that pass through the guide; the dielectric is characterized by a dielectric constant (ε), which is directly proportional to the square of the refractive index of the material. That is;

$$\varepsilon = \varepsilon_0 n^2(x, y) \tag{4.1}$$

where $n(x, y)$ is the refractive index profile.

Figure 4.2 shows the dimensions, the refractive indices and the boundary condition of a straight waveguide as modeled in MEEP software.

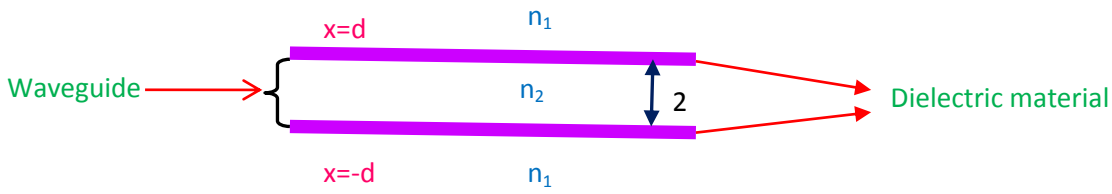

Figure 4.2: waveguide with a dielectric material.

The model in figure 4.3 showing the transmission of power in a straight waveguide as extracted from HDF in MEEP, the frequency source was placed near the left end of the straight waveguide to propagate towards the right.

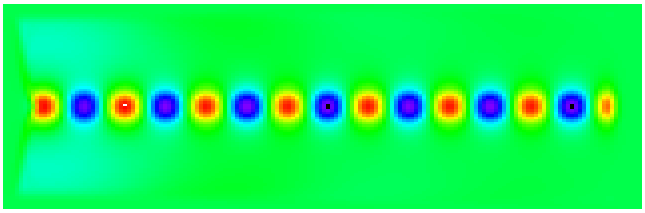

Figure 4.3: waveguide with light of frequency of 0.15 pHz.

When the dielectric of the material which is characterized by Epsilon was increased from 8 – 14 the refractive index increased also, this interfered with the total internal reflection inside the waveguide, leading to power loss in the field. These increases also lead to a phase change/shift in wavelength as seen from an extract of 20 μm - 50

μm from which also there is a downward shift in intensity as the Epsilon was being increased in the waveguide as shown in Figure. 4.4

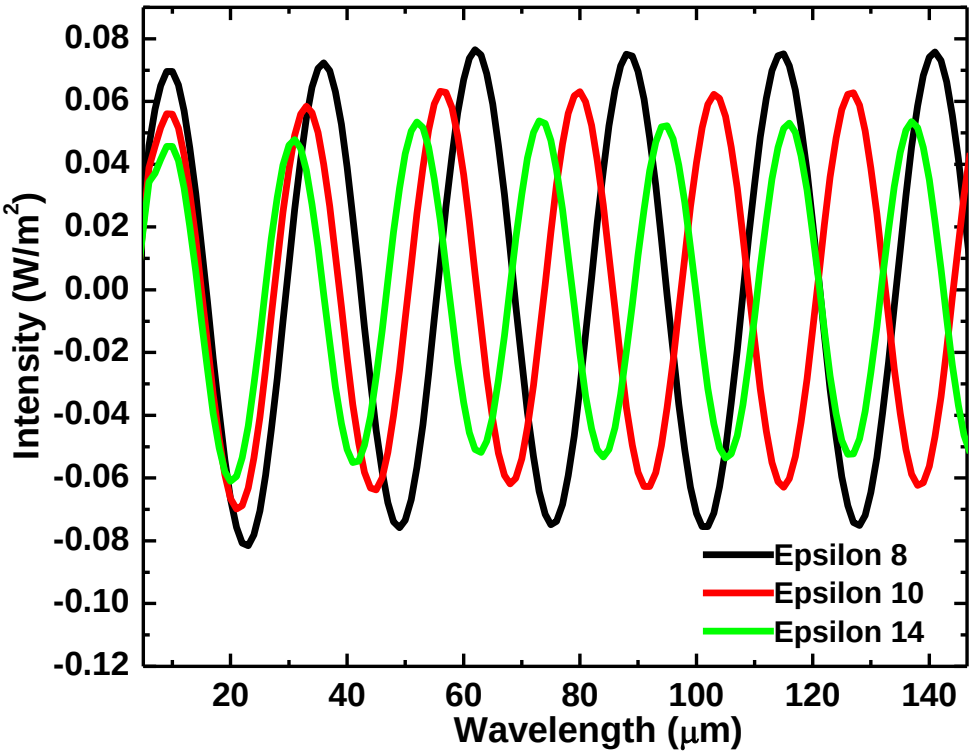

Figure 4.4 : Variation in Intensity and wavelength for a given dielectric constants

When the value of dielectric constant is large the power (intensity as used in MEEP) in the field reduced and when the value of the dielectric constant is small there is more power carried in the field. Since the dielectric constant is proportional to the refractive index, an increase of it confines the fields in the core while decrease of it leads to overlapping of the fields to the cladding regions of the waveguides leading to an increased power; this was in agreement with what is in the literature.

The shifting in the phase of the intensity was reduced when the Epsilon was increased from 12.1 to 12.5, there was also shifting in the phase of wavelength as the Epsilon constant was being increased from 12.1 to 12.5, the graphical representation is as shown in Figure 4.5.

The complex mode amplitudes E_2 are normalized $|E_2|$, which is now equal to overall

power according to equation 2.1.

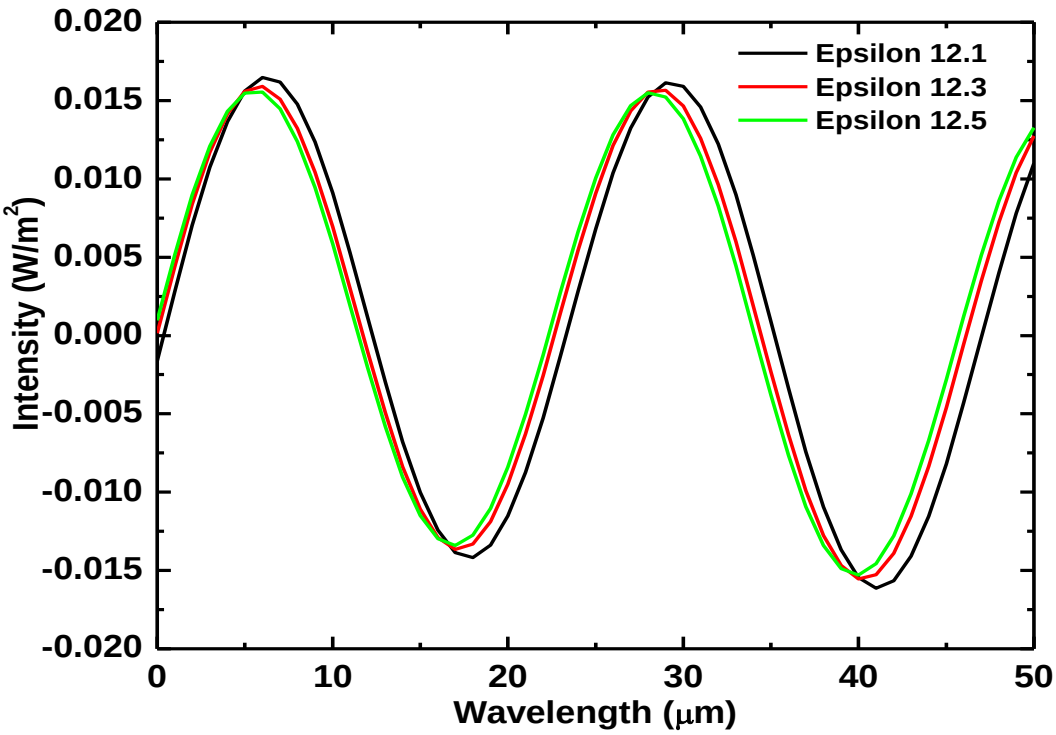

Figure 4.5: Variation in Intensity and wavelength for given dielectric constants

4.3.2 Perfect Matched Layers (PML)

The PML was introduced in the waveguide by the codes in MEEP and were varied from 1 μm to 3 μm so that they don't overlap outside the given cell dimensions, Epsilon was kept constant (ε =12). It was evident that as the thickness increased the intensity reduced as a result of reduced reflections at the PML boundary.

The numerical height of the PML that had minimal interference in the waveguide was in the range of 0.5 μm to 1.5 μm. Again for a given range of wavelength (100 μm – 130 μm) there was also a decrease in intensity as the thickness increased behaving as an attenuator as shown in Figure 4.6.

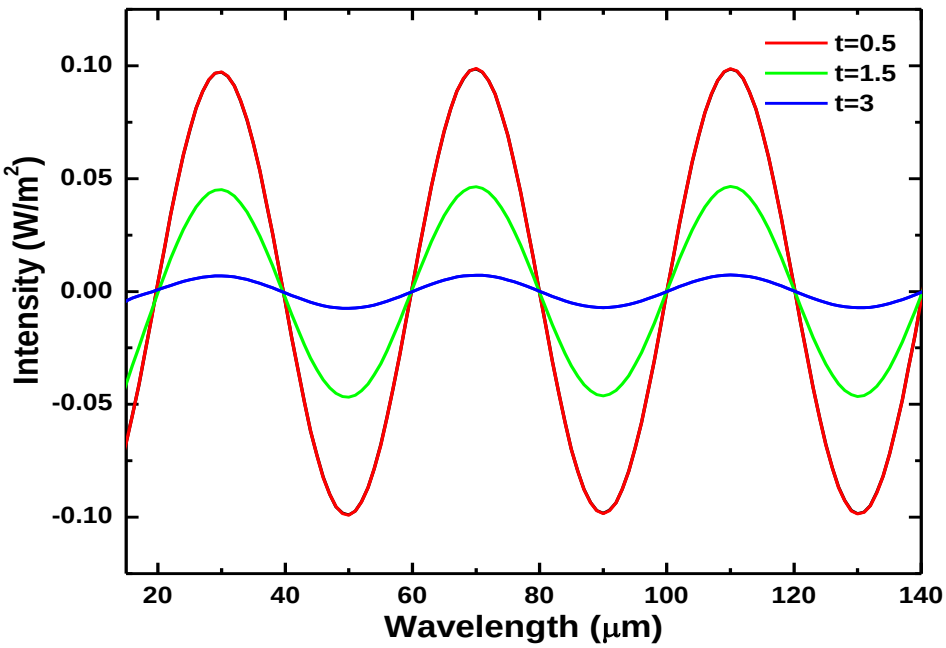

Figure 4.6: Variations in the thickness of PML with Intensity and wavelength.

As the Epsilon value was increased to 12.1 and PML thickness varied from 1.0 μm to 2.0 μm, most of the transmitted power was reduced as a result of interactions with the layers comprising of the PML and the raised Epsilon constant, this is shown in Figure 4.7

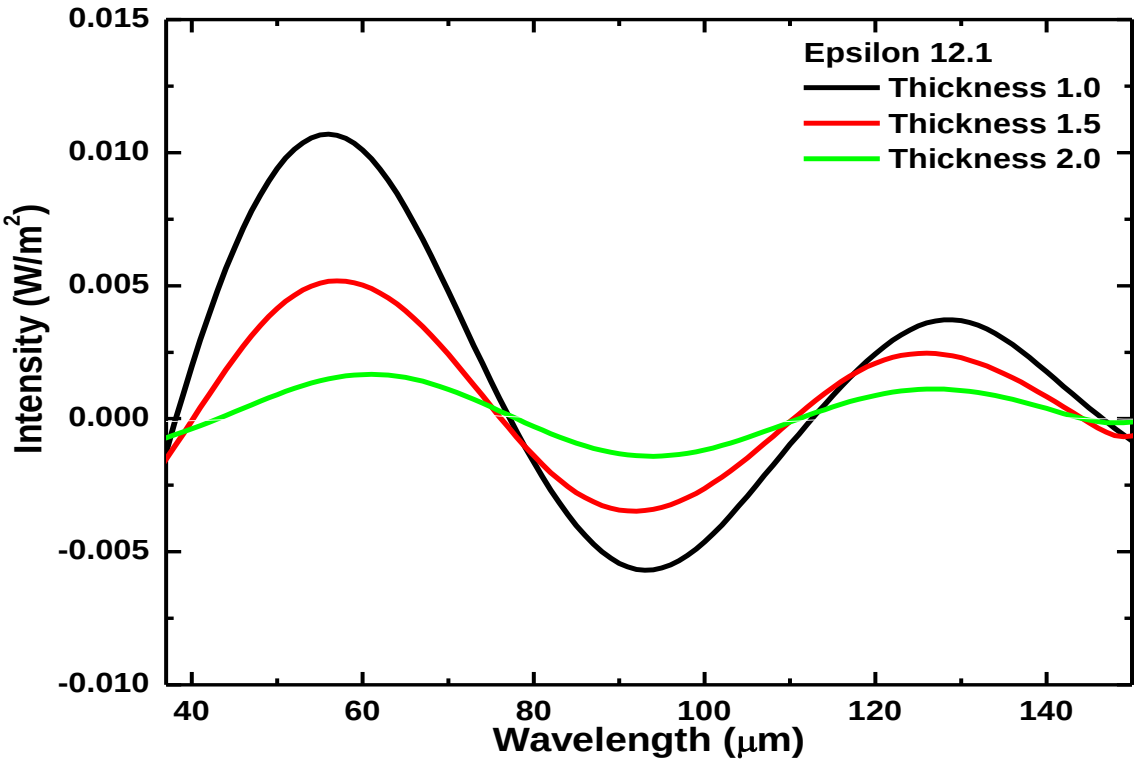

Figure 4.7: Variations in the thickness of PML with Intensity and wavelength

4.3.3 Frequency of the source current

The frequency was varied from 0.1 pHz- 0.25 pHz (Appendix Two) since the target frequency is in this range. As the frequency increase the intensity also increased.

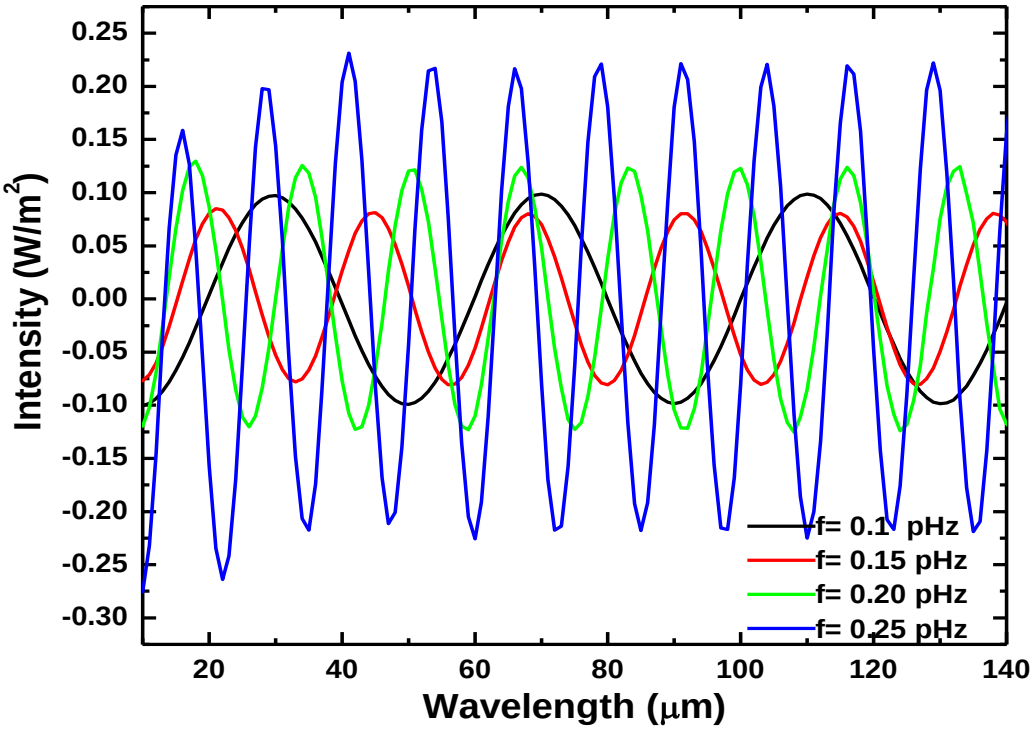

Figure 4.8: Variations in frequency of source current with intensity and wavelength

When the reciprocal of each frequencies 0.1 pHz 0.15 pHz 0.20 pHz and 0.25 pHz are obtained, the periods will be 10 fs, 6.67 fs, 5.0 fs and 4.0 fs respectively; these value corresponds to the period of the wave and because in the MEEP calculation $\varepsilon = 12$, to relate the wavelength with the frequency, Epsilon $\varepsilon = 12$ is then divided by the respective periods giving 1.2, 1.8, 2.4 and 3.0 respectively, this values state how much the wavelength equals to the current source. The value $1.2 \approx 1$ means that the waveguide is roughly equal to the wavelength of the current source, $1.8 \approx 2$ indicate that the waveguide is half the current wavelength, while 2.4 and $3.0 \approx 3$, correspond to a third of the wavelength of the current source.

For frequency values of 0.1 pHz and 0.15 pHz makes the current source to be a single mode and thus the mode is analytically solvable and corresponds to a frequency of 0.15076 pHz as stated in Table 4.1.

4.4 Waveguide with a ring (Notch)

The size of the computation cell used was 160 units in x-direction 160 units in y-direction and zero unit in the z -direction with the center of the first straight waveguide at (-2, -3.5), whose size was infinity in the x-direction, 1 in the y-direction & infinity in the z- direction and the refractive index guide of 3.4. The ring waveguide had its center at (0, 0), who's size was of radius 2.8 μm of infinity height and refractive index of 3.4. The source was a continuous wave of frequency of 0.15 pHz placed at a center (-7, -3.5) whose size was

(0, 1). The running time for the calculation in MEEP was then set to 200 units, to output dielectric constant and electric field along z-axis.

The flow of light from the input at the straight waveguide to the ring and past the ring is shown in Figure 4.9

(a) (b)

Figure 4.9: (a) A notch with no light being transmitted (b) a notch with light being transmitted an extract from HDF.

Light from the source was a broadband as it nears the ring, two things happen; firstly if part of the light is in resonance with the ring its energy will be coupled in the ring and either constructive or destructive interference occurs, most of the power is concentrated in wavelengths between 70 μm to 85 μm since this was the region where

the ring was placed. Secondly, the light that was not at resonance with the ring will not be coupled in the ring but will pass all the way to the through port, this time round with lower amplitude. The power is at maximum where the ring is placed and lowers on either sides of the ring as seen in Figure 4.10.

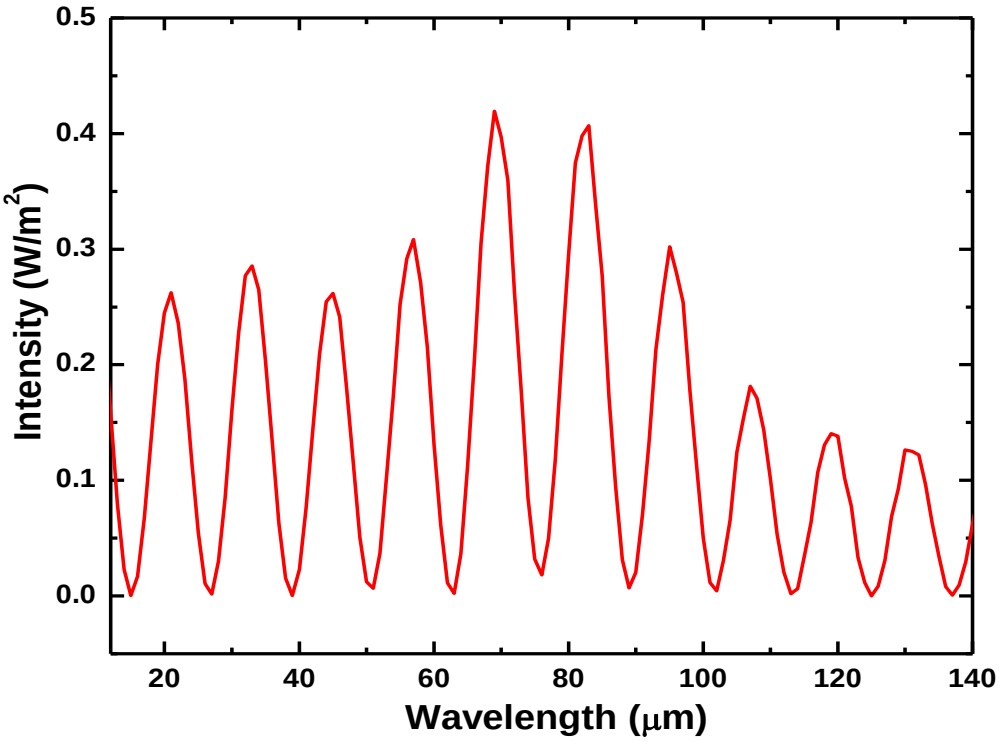

Figure 4.10: Variations in intensity and wavelength from the input port to the throughput port

Power is high inside the ring because of the coupled power from the straight waveguide. Figure 4.11

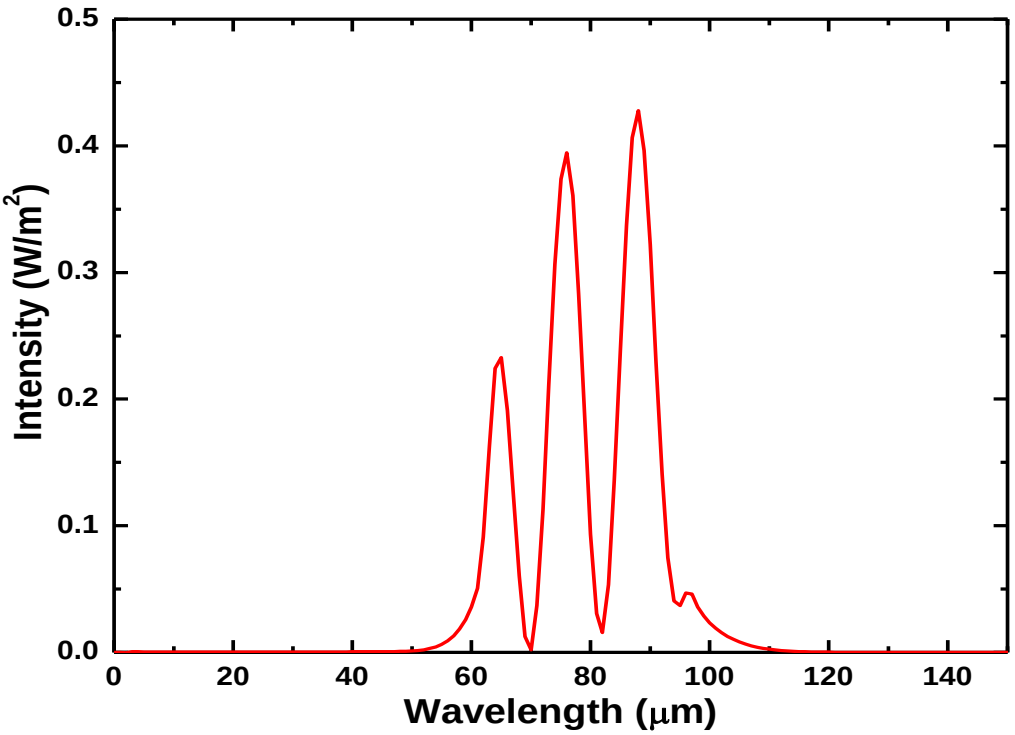

Figure 4.11: Intensity of light Coupled in the Ring at 60 μm 100 μm

The straight waveguide has low power compared to the ring at resonance. This is the characteristic of a filter. The straight waveguide at the input port has some power but at resonance (60 μm to 100 μm) its power drops because some of its energy is transferred to the ring. The energy builds up in the ring due to constructive interference and that is the reason the energy is high (is at peak) in the ring. At the same time when there is no resonance the energy in the straight waveguide is at peak (from 0 μm to 60 μm and from 100 μm to 150 μm) whereas the energy in the ring is low. Figure 4.12 illustrates this

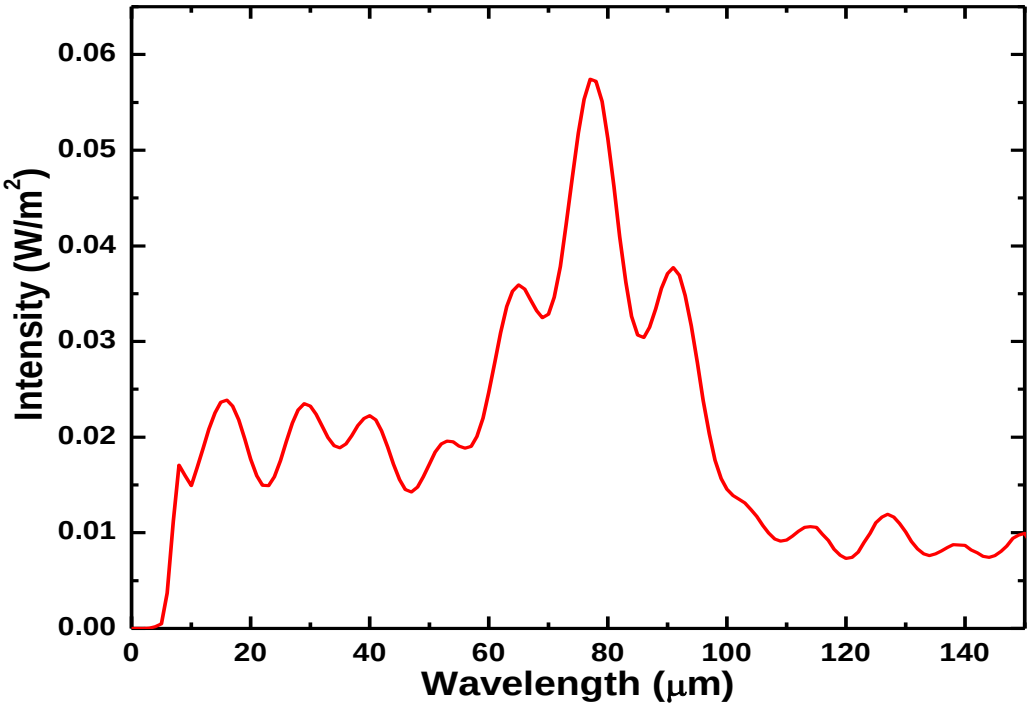

Figure 4.12: Variations of intensity and wavelength at resonance

4.5 Two waveguides with a ring

Here the computation cell was 16 units in x- direction 16 units in y- direction and zero unit in z- direction, size of the waveguides was (infinity 1 infinity) with a width of 1 μm, center (0, -3.8) and (0, 3.8), respectively each of refractive index 3.4. The ring had a radius width of 1 μm, center (0, 0) with a refractive index of 3.4. Continuous wave source frequency of 0.15 pHz size (0, 1) is placed at a center (-7, 3.8). Time run of 200 was used to give an output of different dielectric constants at different and electric field at the end

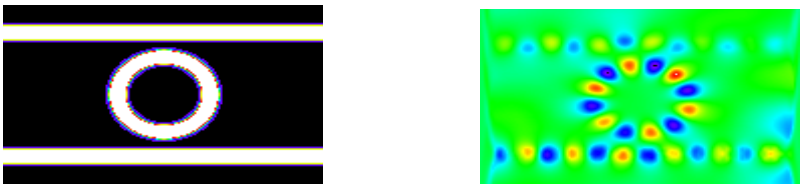

(a) (b)

Figure 4.13: (a) shows a ring resonator with no light (b) a ring resonator with light

The power transmitted in the ring resonator from the input port to the output port has varying amplitude which is high at the center (70 μm) when the ring is at resonance and low elsewhere as shown in Figure 4.14

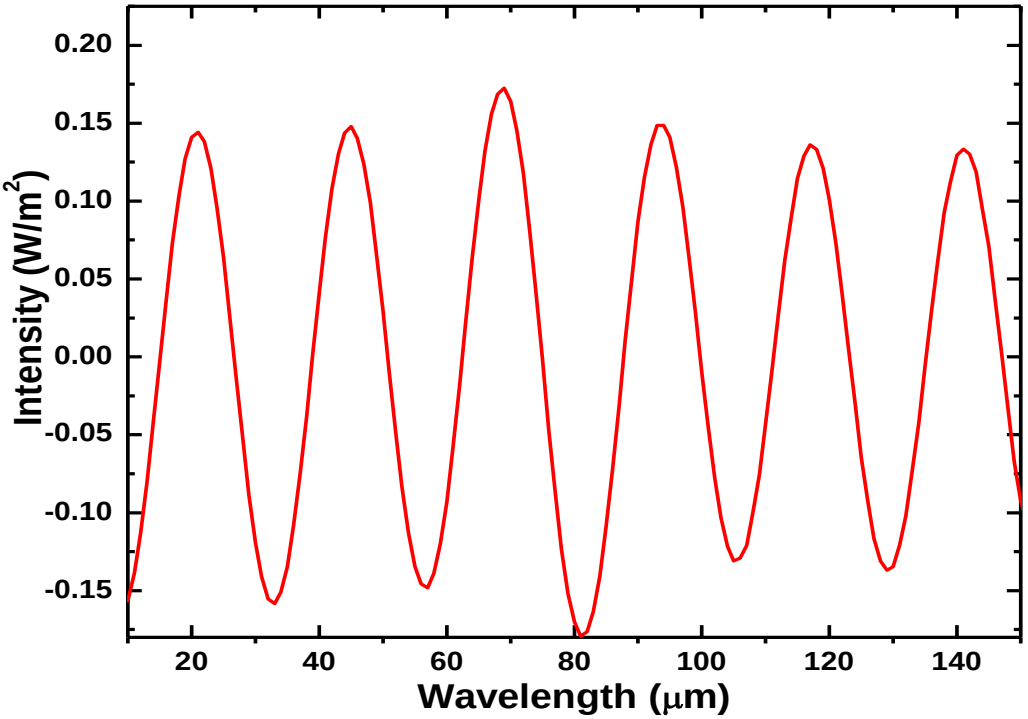

Figure 4.14: Intensity and wavelength in a ring resonator

In the ring power is high at resonance and low further away from it. This is because the power in the loop builds up around trip phase shift; circulating power that equals an integer times 2π, the wave interfere constructively and the cavity goes to resonance as shown in Figure 4.15

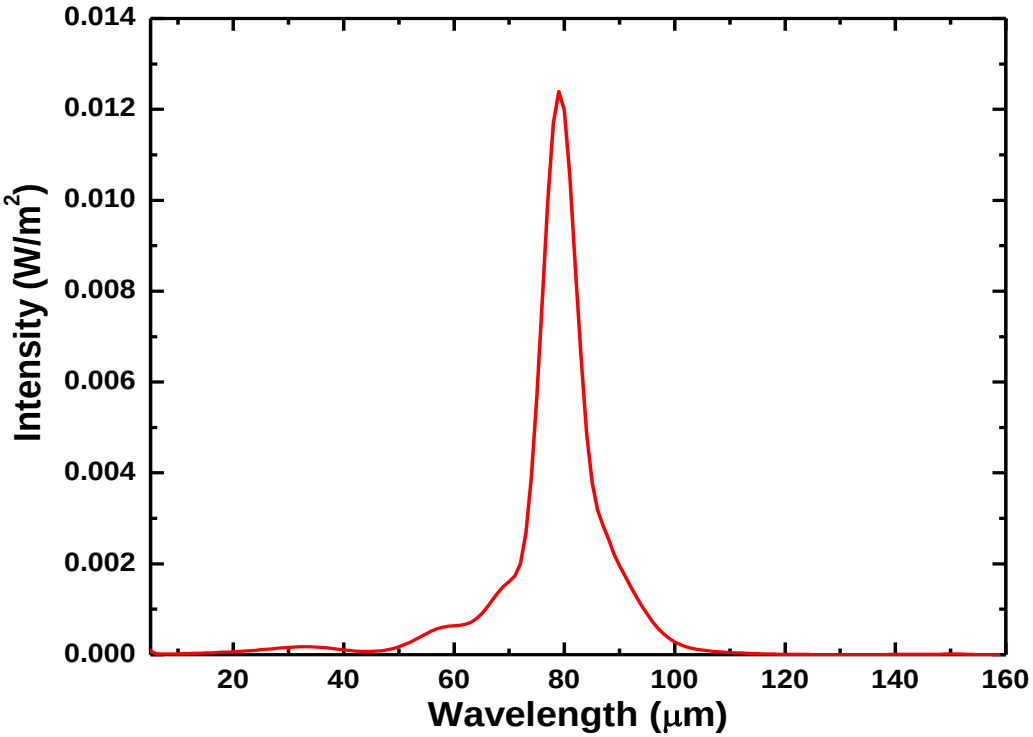

Figure 4.15: Intensity at maximum resonance at 80 μm

4.6 Variation of the distance between the waveguide and the ring

The ring resonator with a ring radius r =2.8 μm and straight waveguide of size infinity in the x –direction, 1 in the y-direction and infinity in the z-direction, both having a refractive index n=3.4 and a width d=1 μm was used. A continuous wave source of frequency f=0.15 pHz placed at point (-7, 3.8) in the lower waveguide. For this broadband source the resonance frequency was found to be in the range

0.068 GHz – 5.026 GHz.

When the gap between the ring and the straight guide was increased by a range of 0.5 μm from an initial 0.5 μm interspace, there was an upward shift in the power that went through the ring at points 54 μm and 104 μm. In this case as the distance is increased the filter characteristics of the optical band pass resonator fades away. This is shown in Figure 4.16

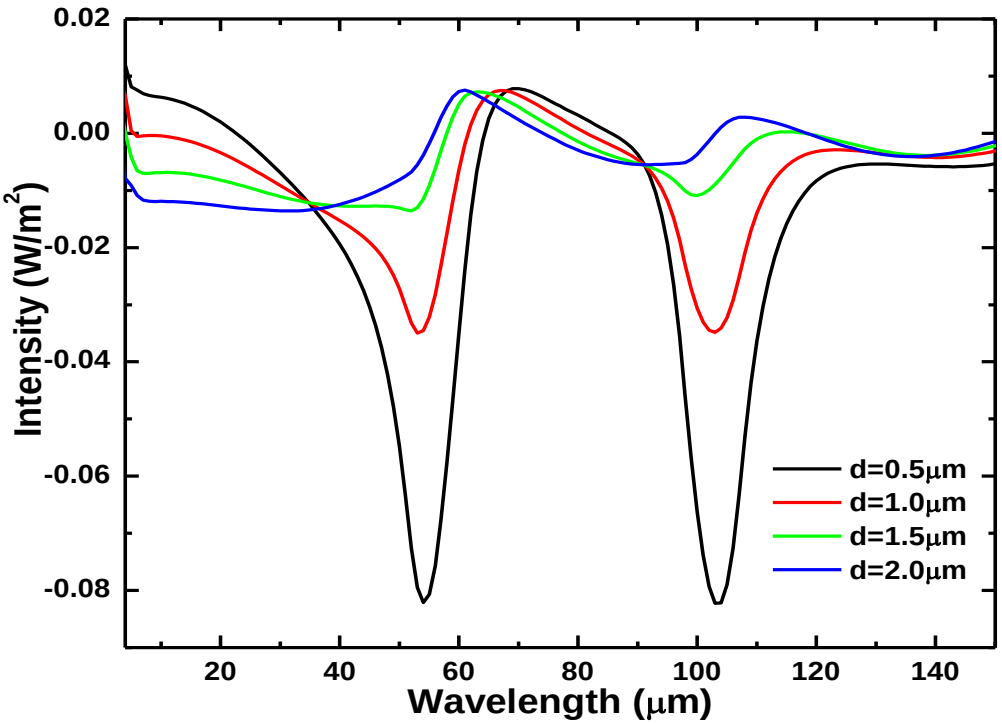

Figure 4.16: Variation in distance d with intensity and wavelength

Specifically the field going to the ring which was between the wavelength of 54 μm and 104 μm, the power that is coupled in the ring increased as the gap between the guide and the ring was minimized because separation gap; d between resonator and waveguides influences the peak width in a way that a wider gap allows achievement of narrower FWHM. This gap was varied from d=0.5 μm to d=0.9 μm. For a minimum of 0.5 μm the power coupled was high; this is presented in the Figure 4.17

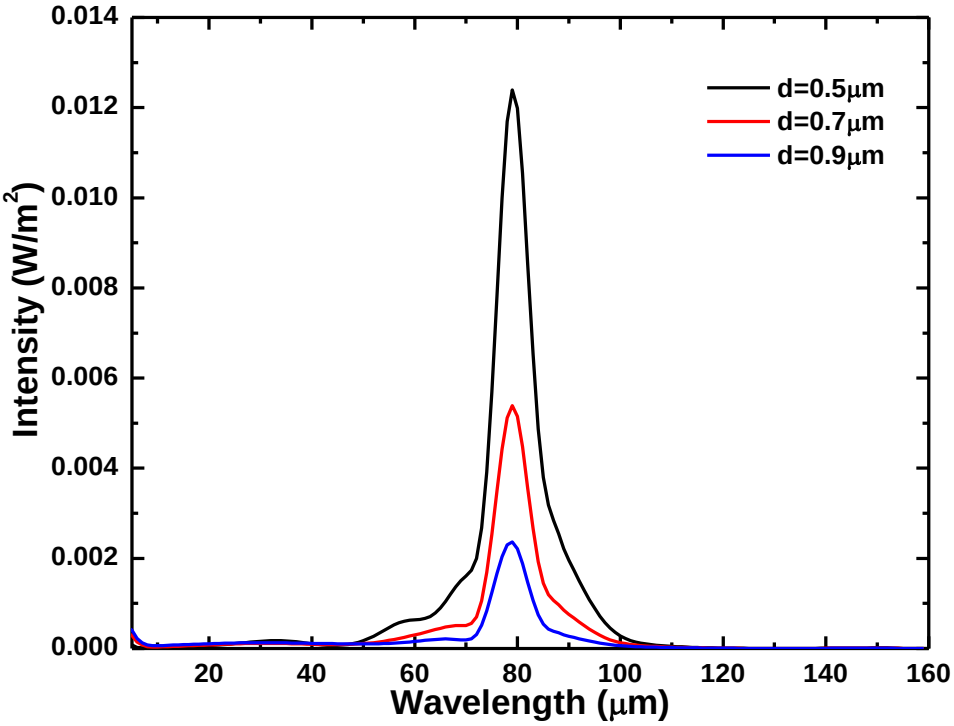

Figure 4.17: Intensity at maximum resonance at 80 μm with varying d.

The power coupled in the ring decreased when the distance was increased from d=0.1 μm to d=0.3 μm. This power was high as compared to Figure 4.17. Also other small peaks were seen as shown in Figure 4.18

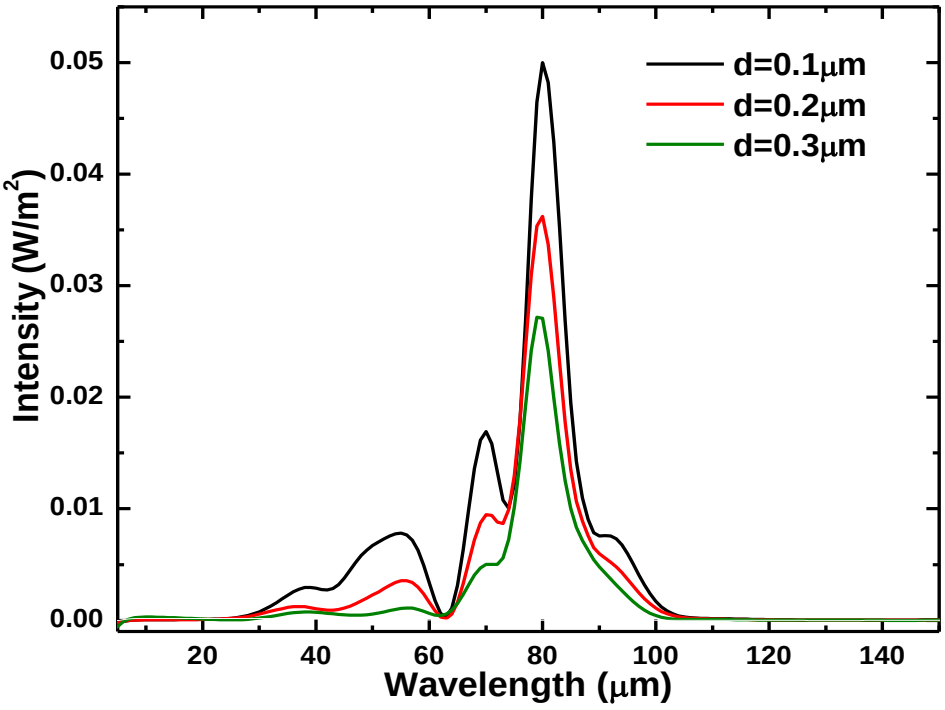

Figure 4.18: Intensity Coupled in the ring with varying distance; d

As the distance d between the ring and the straight waveguide is increased the power coupled into the ring reduced greatly and approached zero. As an indication, distance was varied to a maximum of d=1.5 μm as shown in Figure 4.19

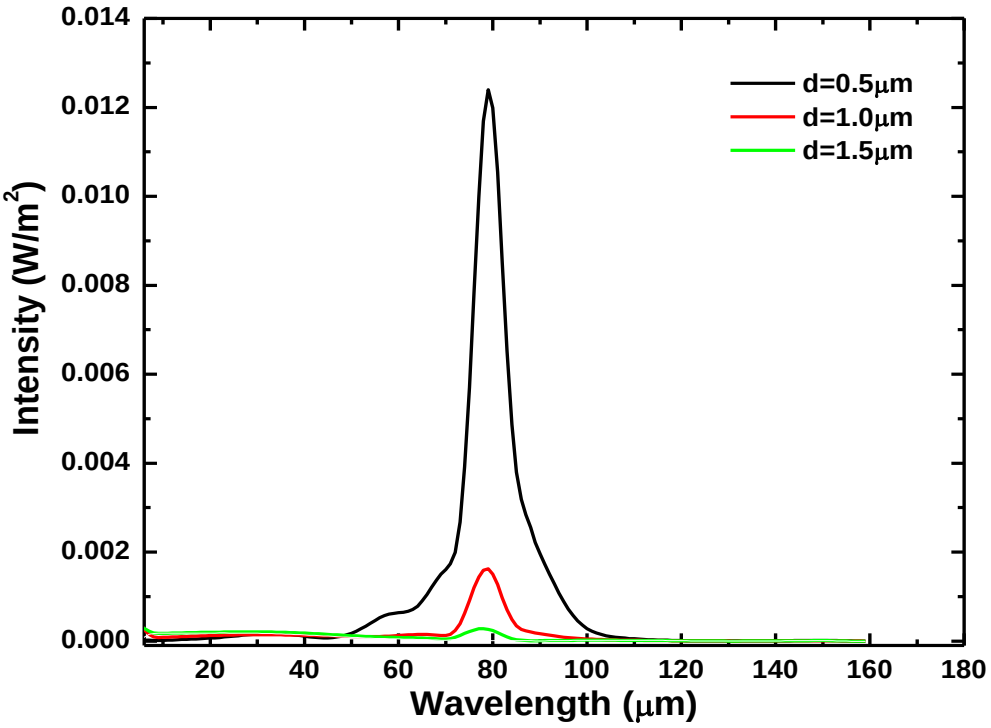

Figure 4.19: variation of the distance d between the ring and the straight guide as intensity changes with wavelength.

4.7 Variation of the computation cell (wavelength Tuning)

Here the computation cell varied from 16x16x0, 24x24x0, 30x30x0 to 36x36x0, however the position of the current source varied from (-7, 3.8), (-11, 3.8), (-14, 3.8) and (-17, 3.8) respectively. The physical parameters were: n=3.4, r=2.8 μm, pulse frequency 0.15, pml=1.0μm and w=1.0 μm. The run time was set at 200.

The results showed a shift in the wavelength with a decrease in the output power. This is the power that is coupled in the ring. In this case a tunable filter was achieved as shown in Figure 4.20

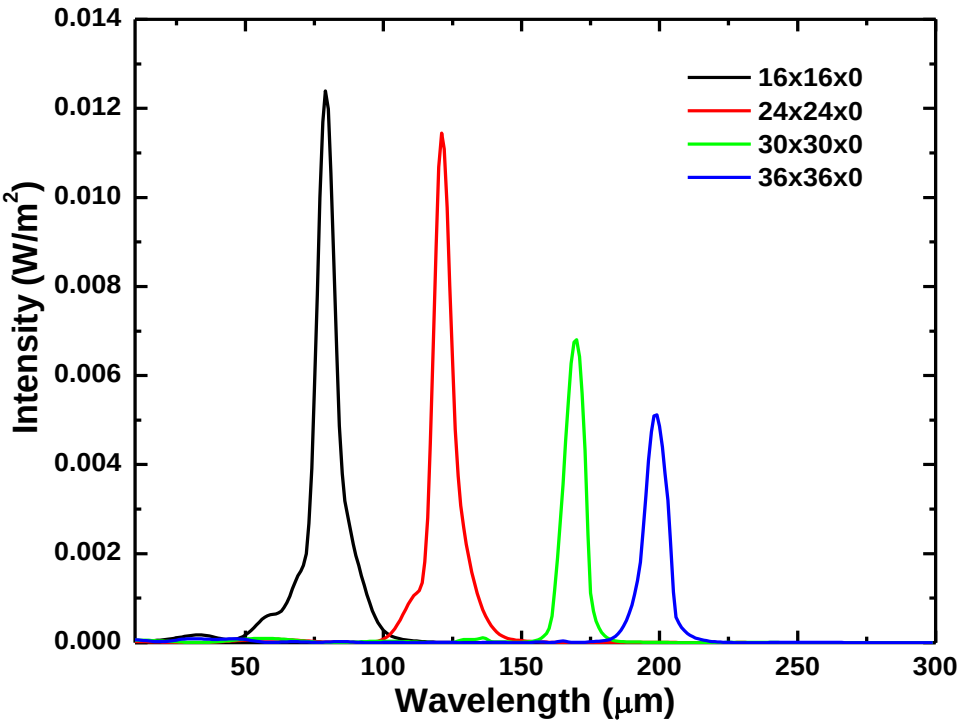

Figure 4.20: different computation cells showing shifting of intensity with wavelength at resonance

4.8 Power variation in different types of Rings

The shifting in the wavelength also arose when the structure of the ring was modified as shown in Figure 4.21. First it was a ring and a single waveguide, second was a ring and two straight waveguides, third was two rings and two straight waveguides and lastly three rings and two waveguides. As the rings were increased the power coupled during resonance kept on reducing because the combination of the rings results to an increase in the structure thus causing higher delays as it takes longer for the power to get into resonance. The outcome is as shown in Figure 4.21 and Figure 4.22

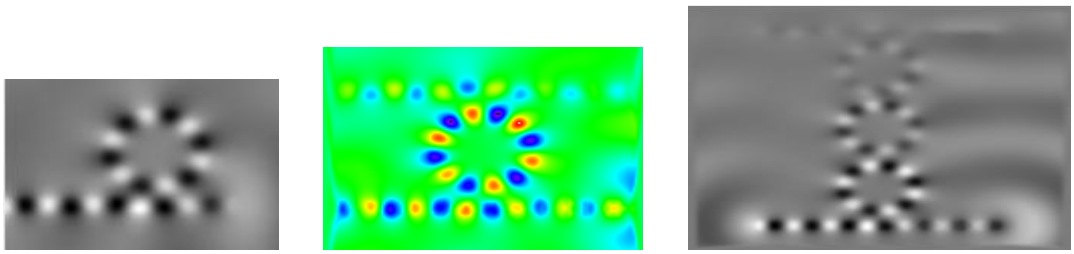

(a) (b). (c)

Figure 4.21: (a) transmission of light in a notch, (b) transmission of light in a resonator with two guides and a ring and (c) transmission of light in a resonator with two guides and three rings

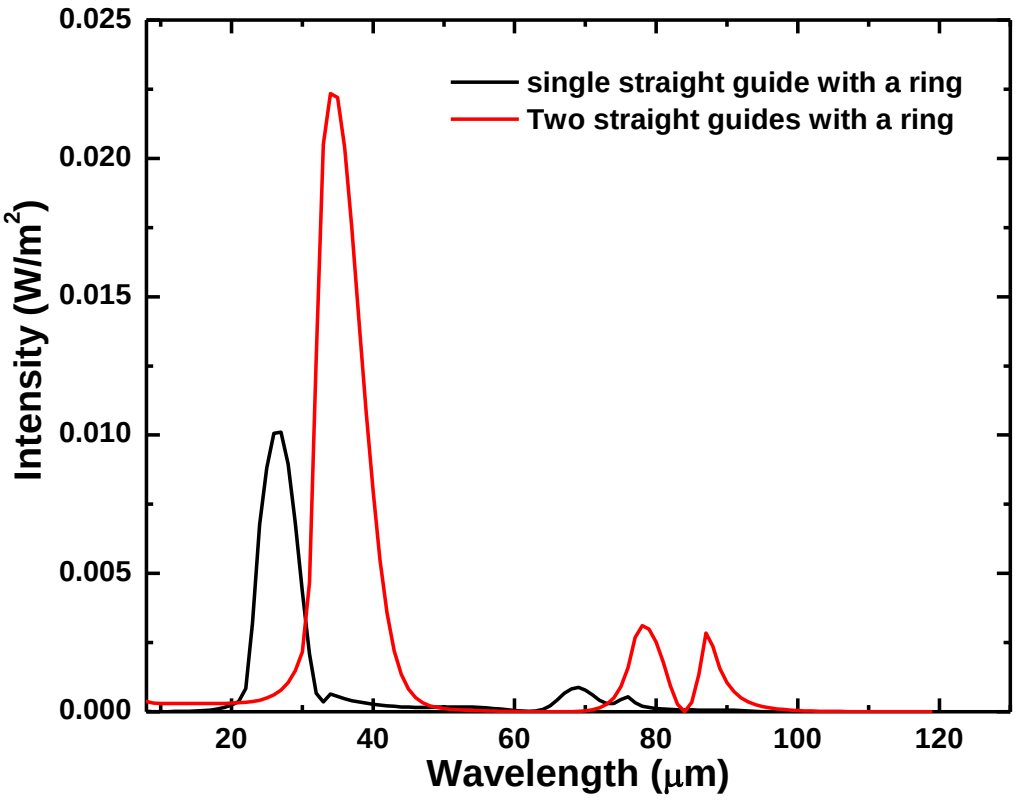

Figure 4.22: shows how shifting in intensity at peaks occurred for both two straight guides with a ring and for two straight guides with three rings.

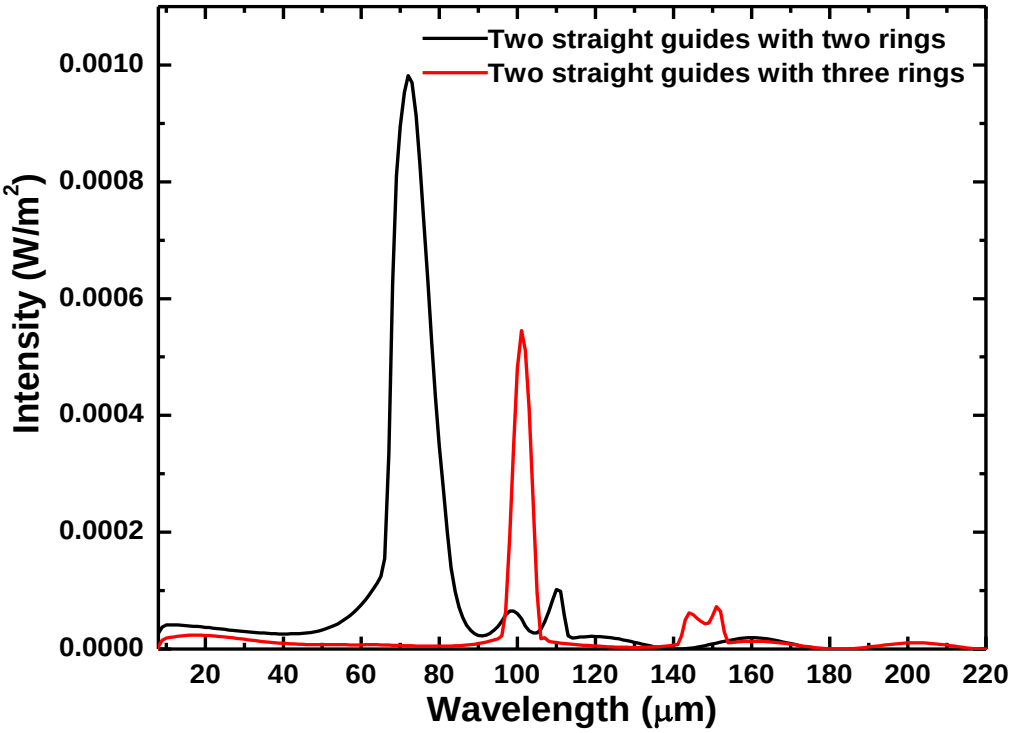

Figure 4.23: Horizontal shifting of intensity and wavelength from double and triple ring resonators at resonance

There was a power comparison for different types of ring resonators after the power goes through the rings, as a result there was amplification of power with maximum power coming from the ring resonator comprising of two waveguides and a single ring as shown in Figure 4.24

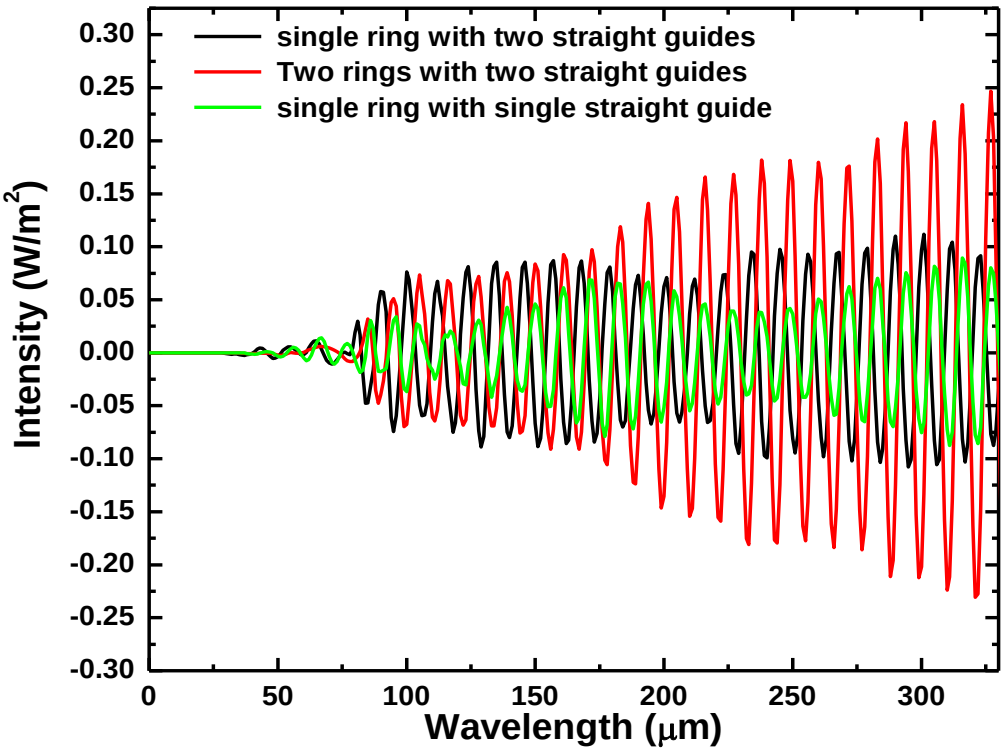

Figure 4.24: Intensity transmission with wavelength for different configurations of ring resonators

CHAPTER FIVE

CONCLUSIONS AND RECOMMENDATIONS

5.1 Conclusions

Demonstration of ring resonators as an optical filter in WDM systems was presented. The validation of analytical analysis using MEEP was carried out in this work with a good agreement. MEEP was able to model Ring resonators that allowed channel filters in WDM.

The ring resonator achieved a resonant frequency of 1.45518×10^{15} rad/s as compared to experimental value of 1.45×10^{15} rad/s and a resonant wavelength of $\lambda=1.2955$ μm as compared to experimental value of $\lambda=1.30$ μm which are the resonant modes for any ring to get into resonance. A single mode of 0.15076 GHz was also achieved as a result of variation in frequency; a factor that affects the Ring resonator.

When the number of rings was increased from a single ring to a double ring and triple ring resonators the coupled power in the ring kept on reducing and causing a horizontal downward shift in the coupled power.

Ring resonators allow for compact channel filters in WDM and represent a key component in modern optical networks. The modeled straight waveguides, Rings of variable radius and different forms of Ring resonators were used to investigate different factors affecting the filter performances, they included Epsilon, Perfect Matched Layers and Frequency.

When the PML and the dielectric constants were increased the power in the waveguides reduced causing a phase shift in the transmission of power as mentioned in Figures 4.4 and 4.6

On the other hand when the size of the computation cell was increased the power that was coupled in the ring reduced, this was a characteristic of a tunable filter though for the decrease in the power a pump could be introduced to amplify the signal.

It was also shown in Figure 4.20 that tunable filter represent a good candidate for add/drop in WDM which will improve the selection of the optical signal and data fibre to home (FTTH).

5.2 Recommendations

This project majorly dealt with a single ring and two straight waveguides however there is need to include several rings arranged in either series or parallel so as to determine the resonant modes and also the response of the filter that is the band rejection and drop losses in MEEP.

Lastly is to model a racetrack resonator and also determine the responses of the same filter in MEEP.

REFERENCES

Agrawal, G. P. (2007). *Nonlinear fiber optics*. Academic press, New York. pp 1-15

Agrawal, G. (2001). *Applications of nonlinear fiber optics*. Academic press, New York Pg 93-115

Akleman, F. & Sevgı, L. (2008). Comparison of Rectangular and Cylindrical FDTD representations on a Ring Resonator Problem. *Turkish Journal of Electrical Engineering & Computer Sciences*, *16*(1).Anderson, G. S. (1979). *U.S. Patent No. 4,143,942*. Washington, DC: U.S. Patent and Trademark Office.

Bates, R. J. (2001). *Optical switching and networking handbook*. McGraw-Hill, Inc.

Berenger, J. 1994. "Aperfectly matched layer for the absorption of electromagnetic waves," *J. Comput. Phys.*, vol. 114, pp. 185–200.

Chaichuay, C., Yupapin, P. P., & Saeung, P. (2009). The serially coupled multiple ring resonator filters and Vernier effect. *Opt. Appl*, *39*, 175-194.

Chew, W. C., & Weedon, W. H. (1994). A 3D perfectly matched medium from modified Maxwell's equations with stretched coordinates. *Microwave and optical technology letters*, *7*(13), 599-604.

Chin, M. K., & Ho, S. T. (1998). Design and modeling of waveguide-coupled single-mode microring resonators. *Journal of Lightwave Technology*, *16*(8), 1433.

Choi, J. M., Lee, R. K., & Yariv, A. (2001). Control of critical coupling in a ring resonatorfiber configuration: application to wavelength-selective switching, modulation, amplification, and oscillation. *Optics letters*, *26*(16), 1236-1238.

Chu, L. J., & Barrow, W. L. (1938). Electromagnetic waves in hollow metal tubes of rectangular cross section. *Radio Engineers, Proceedings of the Institute of, 26*(12), 1520-1555.

Dadashi, K., Kurt, H., Üstün, K., & Esen, R. (2014). Graded index optical microresonators:analytical and numerical analyses. *JOSA B, 31*(9), 2239-2245.

Delâge, A., Xu, D. X., McKinnon, R. W., Post, E., Waldron, P., Lapointe, J., & Schmid, J.H. (2009). Wavelength-dependent model of a ring resonator sensor excited by a directional coupler. *Journal of Lightwave Technology, 27*(9), 1172-1180.

Doerr, C. R., & Kogelnik, H. (2008). Dielectric waveguide theory. *Journal of Lightwave Technology*, *26*(9), 1176-1187.

Ediss, G. A. (2003). ALMA Memo No. 467.

Emerson, D. T. (1997). The work of Jagadis Chandra Bose: 100 years of MM-wave research.*IEEE Transactions on Microwave Theory and Techniques, 45*(12).

Elshoff, M., & Rautenberg, O. (2010). Design and modelling of ring resonators used as optical filters for communications applications.

Elosúa, C., Bariáin, C., Matías, I. R., Arregui, F. J., Luquin, A., Vergara, E., & Laguna, M.(2008). Indicator immobilization on Fabry-Perot nanocavities towards development of fiber optic sensors. *Sensors and Actuators B: Chemical*, *130*(1), 158-163.

Franchimon, E. (2010). Modelling circular optical microresonators using whispering gallery modes (unpublished).

Franchimon, E. F., Hiremath, K. R., Stoffer, R., & Hammer, M. (2013). Interaction of whispering gallery modes in integrated optical microring or microdisk circuits: hybrid coupled mode theory model. *JOSA B*, *30*(4), 1048-1057.

Gambling, W. A. (2000). The rise and rise of optical fibers. *Selected Topics in Quantum Electronics, IEEE Journal of*, *6*(6), 1084-1093.

Gedney, S. 1996. "An anisotropic perfectly matched layer-absorbing medium for the truncation of FDTD lattices," *IEEE Trans. Antennas Propag.*, vol. 44, pp. 1630–1639.

Griffel, G. (2000). Synthesis of optical filters using ring resonator arrays.*IEEE Photonics Technology Letters*, *12*(7), 810-812.

Griffiths, D. J., & Reed College. (1999). *Introduction to electrodynamics* (Vol. 3). Upper Saddle River, NJ: prentice Hall.

Hartig, H. E., & Swanson, C. E. (1938). " Transverse" Acoustic Waves in Rigid Tubes.*Physical Review*, *54*(8), 618.

Hiremath, K. R., Stoffer, R., & Hammer, M. (2005). Multimode circular integrated optical microresonators: Coupled mode theory modeling. *arXiv preprint math-ph/0505079*.

Hodgson, N., & Weber, H. (2005). *Laser resonators and beam propagation*. Springer.

Hopkins, R. (2006, October). Influence of radiation losses in microstrip ring resonators used for materials characterisation. In *IMAPS 39th Int. Symp. Microelectronics* (pp. 65-71).

Kaminow, I., Li, T., & Willner, A. E. (Eds.). (2013). *Optical Fiber Telecommunications Volume VIA: Components and Subsystems*. Academic press.

Khalaj-Amirhosseini, M. (2006). Analysis of coupled nonuniform transmission lines using Taylor's series expansion. *Electromagnetic Compatibility, IEEE Transactions on, 48*(3), 594-600.

Kogelnik, H. (1975). Theory of dielectric waveguides. In *Integrated optics* (pp. 13-81).Springer Berlin Heidelberg.

Kokubun, Y., Hatakeyama, Y., Ogata, M., Suzuki, S., & Zaize, N. (2005). Fabrication technologies for vertically coupled microring resonator with multilevel crossing busline and ultracompact-ring radius. *Selected Topics in Quantum Electronics, IEEE Journal of, 11*(1), 4-10.

Kominato, T., Ohmori, Y., Takato, N., Okazaki, H., & Yasu, M. (1992). Ring resonators composed of GeO 2-doped silica waveguides. *Lightwave Technology, Journal of, 10*(12), 1781-1788.

Ksendzov, A., & Lin, Y. (2005). Integrated optics ring-resonator sensors for protein detection. *Optics letters, 30*(24), 3344-3346.

Lalanne, P., Sauvan, C., & Hugonin, J. P. (2008). Photon confinement in photonic crystal nanocavities. *Laser & Photonics Reviews, 2*(6), 514-526.

Little, B. E., Chu, S. T., Haus, H. A., Foresi, J., & Laine, J. P. (1997). Microring resonator channel dropping filters. *Lightwave Technology, Journal of, 15*(6), 998-1005.

Little, B. E., Foresi, J. S., Steinmeyer, G., Thoen, E. R., Chu, S. T., Haus, H. A., & Greene, W. (1998). Ultra-compact Si-SiO 2 microring resonator optical channel dropping filters. *Photonics Technology Letters, IEEE, 10*(4), 549-551.

Little, B. E., Chu, S. T., Pan, W., & Kokubun, Y. A. K. Y. (2000). Microring resonator arrays for VLSI photonics. *Photonics Technology Letters, IEEE*, *12*(3), 323-325.

Loh, P. R., Oskooi, A. F., Ibanescu, M., Skorobogatiy, M., & Johnson, S. G. (2009).Fundamental relation between phase and group velocity, and application to the failure of perfectly matched layers in backward-wave structures. *Physical Review E*, *79*(6), 065-601.

Magni, V. (1987). Multielement stable resonators containing a variable lens. *JOSA A4*(10), 1962- 1969.

Mansoor, R. D., Sasse, H., Al Asadi, M., Ison, S. J., & Duffy, A. P. (2014). Over coupled ring resonator-based add/drop filters. *Quantum Electronics, IEEE Journal of*, *50*(8), 598-604.

MEEP Tutorials. Retrived, 14th January 2015, from, Ab-initio.mit.edu/wiki/index.php/Meep tutorial

Melloni, A., Carniel, F., Costa, R., & Martinelli, M. (2001). Determination of bend mode characteristics in dielectric waveguides. *Journal of Lightwave Technology*, *19*(4), 571.

Nawrocka, M. S., Liu, T., Wang, X., & Panepucci, R. R. (2006). Tunable silicon microring resonator with wide free spectral range. *Applied physics letters*, *89*(7), 71110-71110.

Okamoto, K. (2010). *Fundamentals of optical waveguides*. Academic press.

Oxborrow, M. (2007). Traceable 2-D finite-element simulation of the whispering gallery modes of axisymmetric electromagnetic resonators. *Microwave Theoryand Techniques, IEEE Transactions on*, *55*(6), 1209-1218.

Photonics, A. (2003). APSS Apollo Application Note on Micro Ring Resonator. *Apollo Inc. Canadá*.

Prkna, L., Čtyroký, J., & Hubálek, M. (2004). Ring microresonator as a photonic structure with complex eigenfrequency. *Optical and Quantum Electronics*, *36*(1-3), 259-269.

Rabiei, P., Steier, W. H., Zhang, C., & Dalton, L. R. (2002). Polymer micro-ring filters and modulators. *Journal of lightwave technology*, *20*(11), 1968.

Rabus, D. G. (2007). *Integrated ring resonators*. Springer-Verlag Berlin Heidelberg.

Ramaswami, R. (2002). Optical fiber communication: from transmission to networking. *IEEE Communications Magazine*, *40*(5), 138-147.

Schmidt, M. A., & Russell, P. S. (2008). Long-range spiralling surface plasmon modes on metallic nanowires. *Optics express*, *16*(18), 13617-13623.

Siegman, A. E. (1986). Lasers University Science Books. *Mill Valley, CA*, *37*.

Snitzer, E., & Osterberg H. (1961). Observed Dielectric Waveguide Modes in the Visible Spectrum< sup>*</sup>. *JOSA*, *51*(5), 499-505.guiding in low index materials using high-index-contrast waveguides. In *MRS Proceedings* (Vol. 797, pp. W6-10). Cambridge University Press.*Communications Magazine, IEEE*, *40*(5), 138-147.

Sobol, H. (1984). Microwave Communications--An Historical Perspective. *Microwave Theory and Techniques, IEEE Transactions on*, *32*(9), 1170-1181.

Stratton, J. A. (2007). *Electromagnetic theory* (Vol. 33). John Wiley & Sons.

Suzuki, S., Oda K., & Hibino, Y. (1995). Integrated-optic double-ring resonators with a wide free spectral range of 100 GHz. *Lightwave Technology, Journal of, 13*(8), 1766-1771.

Tabib-Azar, M., & Beheim, G. (1997). Modern trends in microstructures and integrated optics for communication, sensing, and actuation. *Optical Engineering, 36*(5), 1307-1318.

Thyagarajan, K. S., & Ghatak, A. (2007). *Fiber optic essentials* (Vol. 10). John Wiley & Sons.

Xiao, Y. F., Min, B., Jiang, X., Dong, C. H., & Yang, L. (2008). Coupling whispering gallery-mode microcavities with modal coupling mechanism. *Quantum Electronics, IEEE Journal of, 44*(11), 1065-1070.

Xu, Q., Fattal, D., & Beausoleil, R. G. (2008). Silicon microring resonators with 1.5-μm radius. *Optics express*, *16*(6), 4309-4315.

Yariv, A. (1973). Coupled-mode theory for guided-wave optics. *Quantum Electronics, IEEE Journal of, 9*(9), 919-933.

Yariv, A. (2000). Universal relations for coupling of optical power between microresonators and dielectric waveguides. *Electronics letters, 36*(4), 321-322.

Yariv, A. (2002). Critical coupling and its control in optical waveguide-ring resonator systems. *IEEE Photonics Technology Letters, 14*(4), 483-485.

Yee, K. S. (1966). Numerical solution of initial boundary value problems involving Maxwell's equations in isotropic media. *IEEE Trans. Antennas Propag, 14*(3), 302-307.

Zhang, X. Y., & Xue, Q. (2007). Novel dual-mode dual-band filters using coplanar waveguide-fed ring resonators. *Microwave Theory and Techniques, IEEE Transactions on*, *55*(10), 2183-2190.

Zhang, Z., & Satpathy, S. (1990). Electromagnetic wave propagation in periodic structures: Bloch wave solution of Maxwell's equations. *Physical review letters*, *65*(21), 2650.

Zhao, L. and Cangellaris, A. C., 1996. "GT-PML: Generalized theory of perfectly matched layers and its application to the reflectionless truncation of finite-difference timedomain grids," *IEEE Trans. Microw. Theory Tech.*, vol. 44, pp. 2555–2563.

APPENDIX A

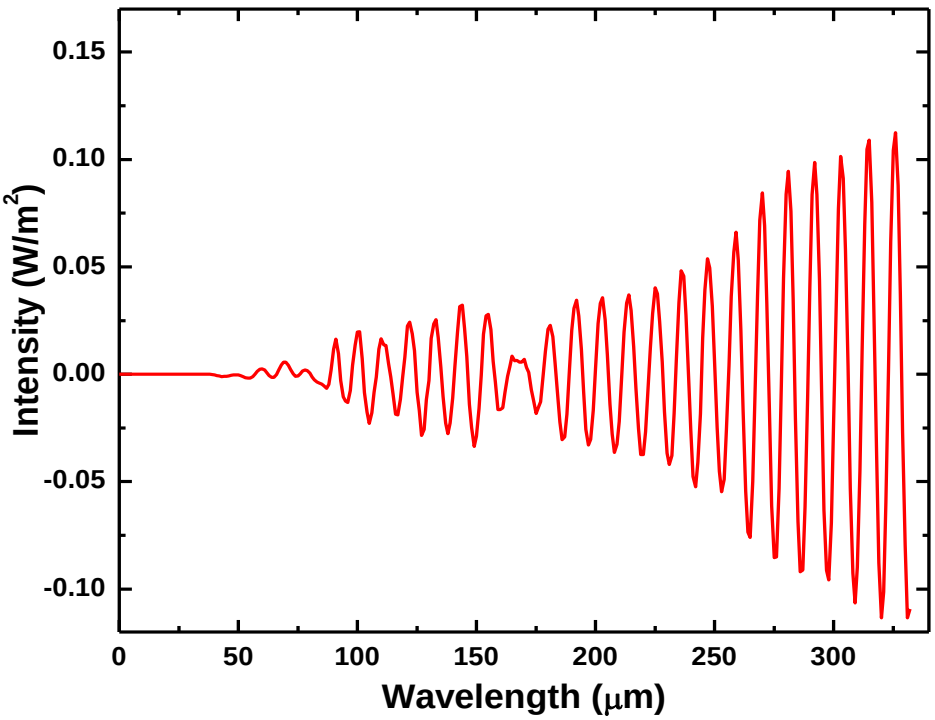

Appendix A 1: Light transmission in a ring resonator

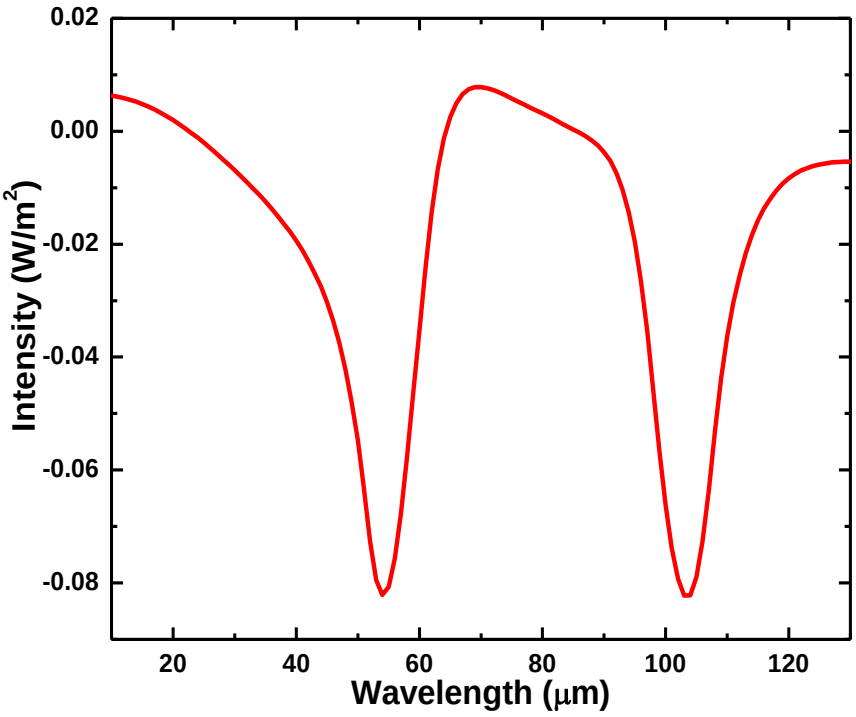

Appendix A 2: Filter characteristics of a ring resonator

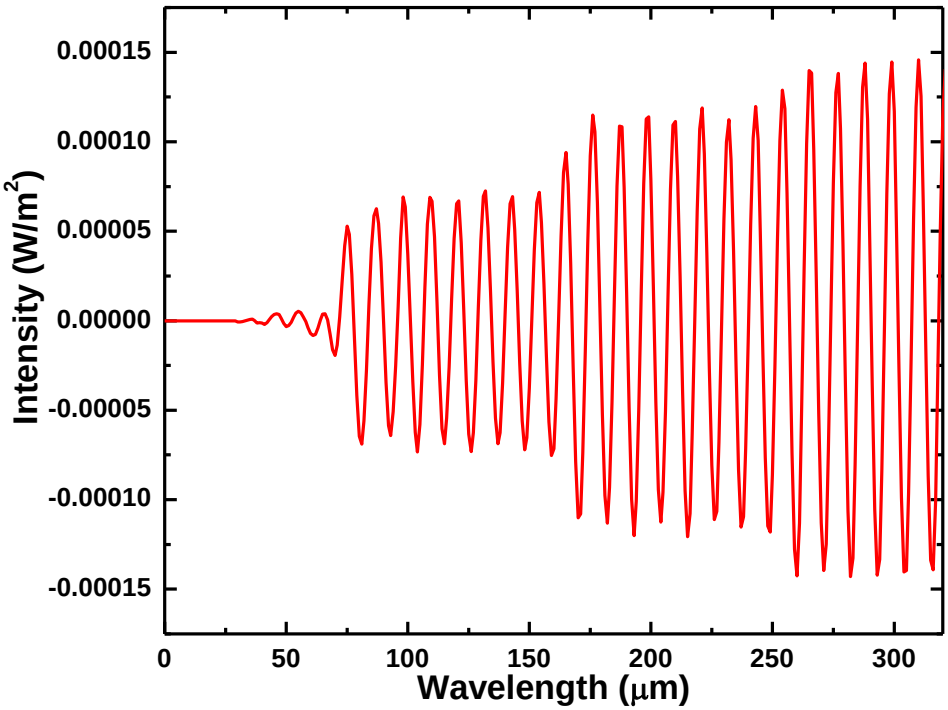

Appendix A 3: Light transmission at different time step in a ring resonator

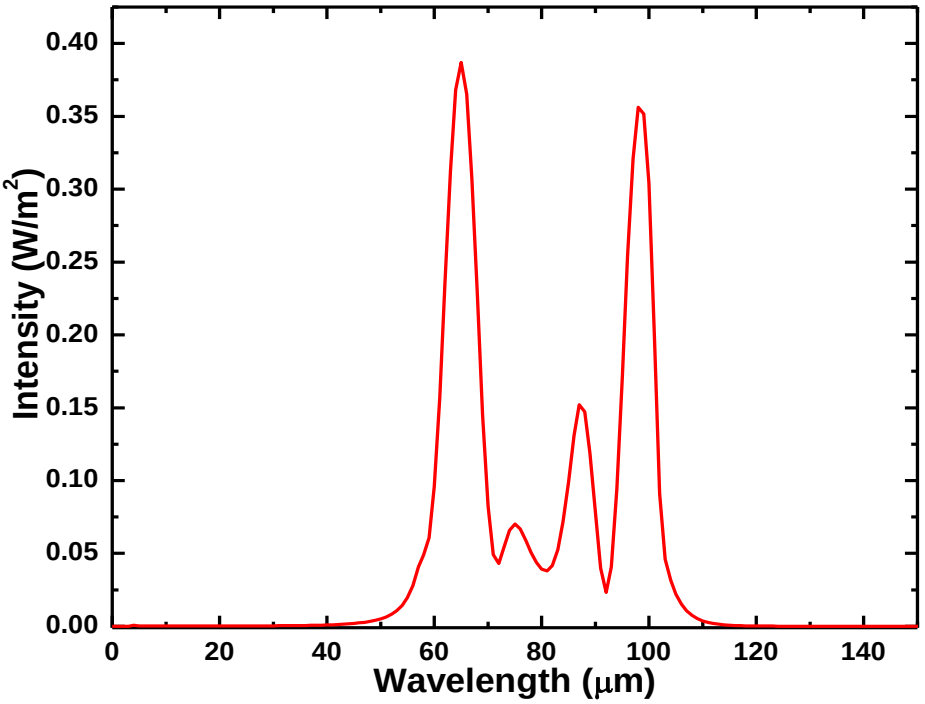

Appendix A 4: Light at resonance in a ring resonator

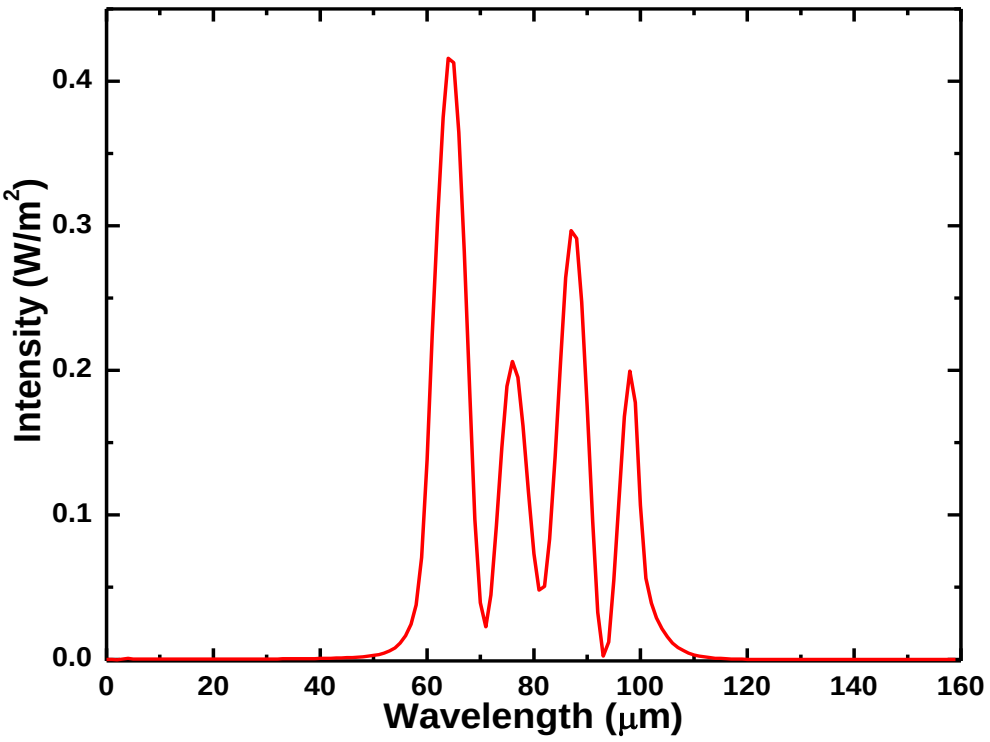

Appendix A 5: Light at resonance at different time step in a ring resonator

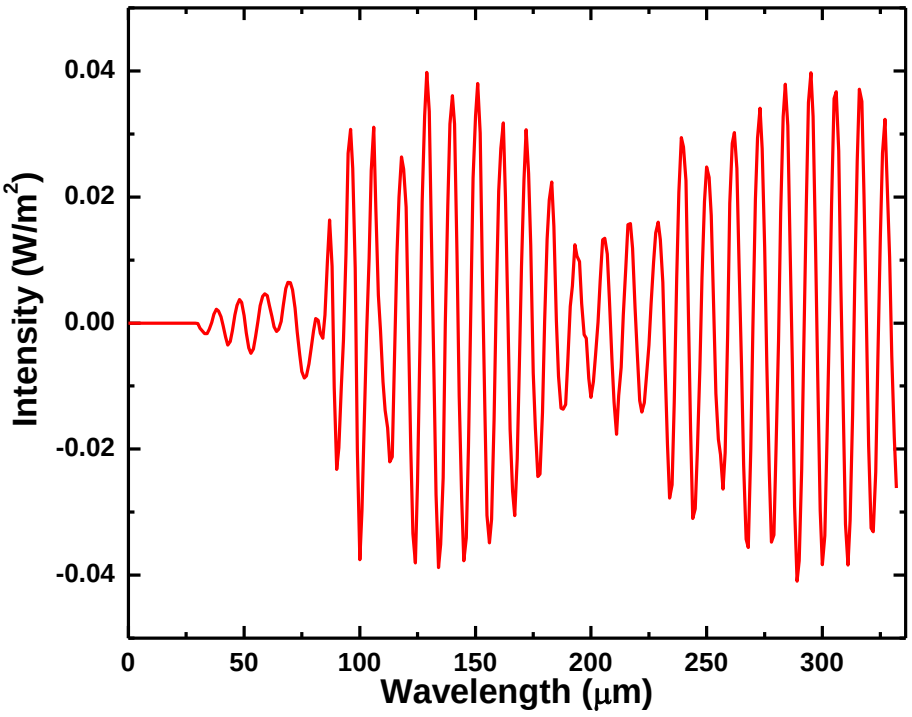

Appendix A 6: Light transmission at different time step in a ring resonator

APPENDIX B

A.1 Presentations

1. Research and innovation for sustainable development- University of Eldoret, 18th – 19th June 2015

2. Modeling of Ring Resonators for Optical Filters Applications using MEEP was accepted for Publications at International Journal of Emerging Technology and Advanced Engineering (ISSN 2250-2459, ISO 9001:2008 Certified Journal, Volume 5, Issue 9, September 2015).

3. 2016 International Conference on Sustainable Research and Innovation – Kenya School of Monetary Studies, 4th -6th May 2016. http:// www.jkuatsri.com/ ojs/index.php/ proceedings /article/ view/407/286.